Domain-specific Quantification of Prion Protein in Cerebrospinal Fluid by Targeted Mass Spectrometry

Authors

Eric Vallabh Minikel, Eric Kuhn, Alexandra R. Cocco, Sonia M. Vallabh, Christina R. Hartigan, Andrew G. Reidenbach, Jiri G. Safar, Gregory J. Raymond, Michael D. McCarthy, Rhonda O'Keefe, Franc Llorens, Inga Zerr, Sabina Capellari, Piero Parchi, Stuart L. Schreiber, and Steven A. Carr

Correspondence

eminikel@broadinstitute.org;
scarr@broad.mit.edu

Graphical Abstract

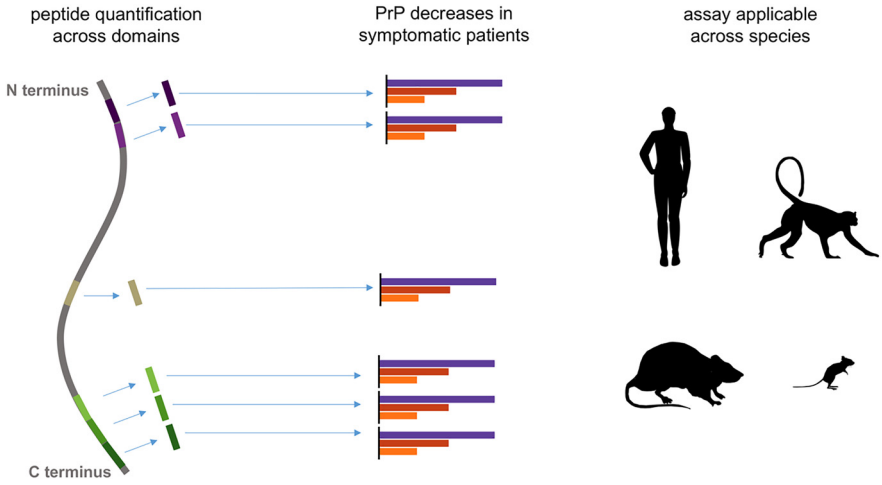

In Brief

PrP in cerebrospinal fluid is measured by targeted mass spectrometry using peptides across protein domains in humans and preclinical species of interest. Peptides are uniformly reduced in patients with prion disease, suggesting that dose-finding studies of PrP-lowering drugs may be most informative in presymptomatic individuals.

Highlights

- Targeted mass spectrometry assay to quantify prion protein (PrP) in spinal fluid.
- Precise measurement of PrP peptide concentration across protein domains.
- Peptides are uniformly decreased in symptomatic prion disease patients.
- Assay applicable to humans and preclinical species for drug development.

Minikel et al., 2019, Molecular & Cellular Proteomics *18*, 2388–2400
December 2019 © 2019 Minikel et al. Published under exclusive license by The American Society for Biochemistry and Molecular Biology, Inc.
https://doi.org/10.1074/mcp.RA119.001702

Domain-specific Quantification of Prion Protein in Cerebrospinal Fluid by Targeted Mass Spectrometry*[S]

Eric Vallabh Minikel‡§¶‡‡‡‡§§§§, Eric Kuhn‖§§§§, Alexandra R. Cocco‖, Sonia M. Vallabh‡§¶, Christina R. Hartigan‖, Andrew G. Reidenbach‡, Jiri G. Safar**, Gregory J. Raymond‡‡, Michael D. McCarthy§§, Rhonda O'Keefe§§, Franc Llorens¶¶‖‖‖‖, Inga Zerr¶¶, Sabina Capellari‡‡‡§§§, Piero Parchi‡‡‡¶¶¶, Stuart L. Schreiber‡‖‖‖‖, and Steven A. Carr‖¶¶¶¶

Therapies currently in preclinical development for prion disease seek to lower prion protein (PrP) expression in the brain. Trials of such therapies are likely to rely on quantification of PrP in cerebrospinal fluid (CSF) as a pharmacodynamic biomarker and possibly as a trial endpoint. Studies using PrP ELISA kits have shown that CSF PrP is lowered in the symptomatic phase of disease, a potential confounder for reading out the effect of PrP-lowering drugs in symptomatic patients. Because misfolding or proteolytic cleavage could potentially render PrP invisible to ELISA even if its concentration were constant or increasing in disease, we sought to establish an orthogonal method for CSF PrP quantification. We developed a multispecies targeted mass spectrometry method based on multiple reaction monitoring (MRM) of nine PrP tryptic peptides quantified relative to an isotopically labeled recombinant protein standard for human samples, or isotopically labeled synthetic peptides for nonhuman species. Analytical validation experiments showed process replicate coefficients of variation below 15%, good dilution linearity and recovery, and suitable performance for both CSF and brain homogenate and across humans as well as preclinical species of interest. In $n = 55$ CSF samples from individuals referred to prion surveillance centers with rapidly progressive dementia, all six human PrP peptides, spanning the N- and C-terminal domains of PrP, were uniformly reduced in prion disease cases compared with individuals with nonprion diagnoses. Thus, lowered CSF PrP concentration in prion disease is a genuine result of the disease process and not an artifact of ELISA-based measurement. As a result, dose-finding studies for PrP lowering drugs may need to be conducted in presymptomatic at-risk individuals rather than in symptomatic patients. We provide a targeted mass spectrometry-based method suitable for preclinical quantification of CSF PrP as a tool for drug development. ***Molecular & Cellular Proteomics 18: 2388–2400, 2019. DOI: 10.1074/mcp.RA119.001702.***

Prion disease is a fatal and incurable neurodegenerative disease caused by misfolding of the prion protein[1] (PrP), and may be sporadic, genetic, or acquired (1). Therapies currently in preclinical development for prion disease seek to lower PrP levels in the brain, a genetically well-validated strategy (2). Clinical trials of PrP-lowering agents will rely on quantification of PrP in cerebrospinal fluid (CSF) as, at a minimum, a pharmacodynamic biomarker (3). This marker may, however, have even greater importance. Predictive testing of presymptomatic individuals harboring highly penetrant genetic mutations (4) that cause prion disease provides an opportunity for early therapeutic intervention to preserve healthy life, but randomization to a clinical endpoint in this population appears infeasible (5). The U.S. Food and Drug Administration has indicated its willingness to consider lowered CSF PrP in this population as a potential surrogate endpoint for Accelerated Approval (6, 7). Precise quantification of PrP in CSF will be essential to the development of prion disease therapeutics.

From the ‡Chemical Biology and Therapeutics Science Program, ‖Proteomics Platform, §§Environmental Health and Safety, Broad Institute of MIT and Harvard, Cambridge, MA 02142; §Program in Biological and Biomedical Sciences, Harvard Medical School, Boston, MA 02115; ¶Prion Alliance, Cambridge, MA 02139; **Departments of Pathology and Neurology Case Western Reserve University, Cleveland, OH 44106; ‡‡Laboratory of Persistent Viral Diseases, NIAID Rocky Mountain Labs, Hamilton, MT 59840; ¶¶National Reference Center for TSE, Georg-August University, Göttingen, 37073, Germany; ‖‖‖‖Biomedical Research Networking Center on Neurodegenerative Diseases (CIBERNED), L'Hospitalet de Llobregat, 08908, Barcelona, Spain; ‡‡‡IRCCS Istituto delle Scienze Neurologiche di Bologna, Bologna, 40139, Italy; §§§Department of Biomedical and Neuromotor Sciences, University of Bologna, Bologna, 40123, Italy; ¶¶¶Department of Experimental, Diagnostic and Specialty Medicine, University of Bologna, Bologna, 40138, Italy; ‖‖‖‖‖Department of Chemistry & Chemical Biology, Harvard University, Cambridge, MA 02138

Received July 29, 2019, and in revised form, September 16, 2019
Published, MCP Papers in Press, September 26, 2019, DOI 10.1074/mcp.RA119.001702

PrP is an extracellular GPI-anchored protein that can be shed from the plasma membrane by ADAM10 and other peptidases (8, 9). CSF PrP is predominantly soluble and full-length (10), suggesting that it originates chiefly from this proteolytic shedding near the C terminus, although lower molecular weight fragments of PrP have also been identified in CSF (11), which may originate from other endoproteolytic events (8, 12), and anchored PrP is also released from cells on exosomes (13). PrP is sufficiently abundant in CSF, at concentrations of tens or hundreds of nanograms per milliliter, to be readily quantified with enzyme-linked immunosorbent assay (ELISA). Studies using ELISA have reproducibly found that CSF PrP is decreased in the symptomatic phase of prion disease (3, 14–17). Therefore, even though CSF PrP is brain-derived and exhibits good within-subject test-retest reliability in individuals without prion disease (3), it might be difficult to use this biomarker to read out the effect of a PrP-lowering drug in symptomatic individuals, because it is unclear whether to expect that such a drug should cause a further decrease in CSF PrP as a direct pharmacodynamic effect, or an increase in CSF PrP because of alleviation of the disease process. This confounder could potentially limit the use of ELISA-based CSF PrP quantification as a pharmacodynamic biomarker to presymptomatic individuals only.

Prion disease is caused by a gain of function (1), and animal studies have shown that total PrP in the brain increases over the course of prion disease as misfolded PrP accumulates (18–20). The paradoxical decrease in PrP in CSF during prion disease might be because of its incorporation into plaques (21), diversion into intracellular locations (22, 23), or down-regulation as a function of the disease process (24). However, although the ELISA assay has been described as measuring "total PrP," the assay's reactivity for different conformations or proteolytic fragments of PrP has not been evaluated, leaving doubt as to what the disease-dependent reduction in CSF PrP means. Occlusion of epitopes because of misfolding (25) or up-regulation of proteolytic cleavage in disease (8, 24, 26) could render PrP invisible to ELISA even if its concentration were constant or increasing. We therefore sought to establish an orthogonal method for CSF PrP quantification. In addition, because the commercially available ELISA kit is specific to human PrP (3), we required a multi-species assay applicable to the preclinical phases of drug development.

Here, we describe quantification of CSF PrP relative to an isotopically labeled recombinant protein standard using multiple reaction monitoring mass spectrometry (MRM-MS) (27). We analyze $n = 55$ clinical samples from prion and nonprion disease patients, and find that six out of six PrP tryptic peptides, spanning N- and C-terminal domains of the protein, are uniformly decreased in prion disease. Thus, PrP concentration is genuinely lowered in prion disease CSF, meaning that dose-finding studies for PrP-lowering drugs may need to be conducted in presymptomatic individuals. To provide similar capability to measure drug-dependent changes in PrP concentration in tissues from preclinical species of interest, we also developed assays for mouse, rat, and cynomolgus macaque based on quantification relative to isotopically labeled synthetic peptide standards. Our findings supply an alternative method for validating the findings of ELISA-based studies of CSF PrP, and provide a potential assay for use as a pharmacodynamic biomarker in preclinical drug development and in human trials.

EXPERIMENTAL PROCEDURES

Experimental Design and Statistical Rationale—We designed this study to compare the levels of PrP tryptic peptides in CSF samples from individuals referred for diagnostic testing for prion disease, later determined to have prion disease (cases, $n = 34$) or not (controls, $n = 21$), details provided in next section. We selected this set of CSF samples because we had previously analyzed them by ELISA and found that the difference in "total PrP" level between cases and controls was highly significant ($p = 0.0001$), suggesting our analysis should be well-powered to replicate or refute the ELISA findings. Operators were blinded to case/control status and samples were randomly assigned to different analysis days using an R script. Each sample was analyzed in duplicate and the mean value for each peptide from two replicates was used. Data were analyzed primarily by visual inspection and the use of confidence intervals. Because our study was limited to examining previously reported hypotheses, and not exploring new ones, p values are nominal where reported.

Cerebrospinal Fluid and Brain Samples—This study was approved by the Broad Institute's Office of Research Subjects Protection (ORSP-3587). Written consent for research use of samples was obtained from patients or next of kin as appropriate.

All CSF samples in this study have been previously reported (3). CSF samples for assay development were large volume normal pressure hydrocephalus samples provided by MIND Tissue Bank at Massachusetts General Hospital. Clinical CSF samples ($n = 55$) were premortem lumbar punctures from rapidly progressive dementia patients referred to prion surveillance centers in Italy (Bologna) or Germany (Göttingen) with suspected prion disease and who were later either determined by autopsy or probable diagnostic criteria (28) including real-time quaking-induced conversion (RT-QuIC (29)) as prion disease, or confirmed as nonprion cases on the basis of autopsy, patient recovery, or definitive other diagnostic test. Individuals with nonprion diagnoses ($n = 21$) included autoimmune disease ($n = 8$), nonprion neurodegenerative disease ($n = 6$), psychiatric illness ($n = 3$), stroke ($n = 1$), brain cancer ($n = 1$), and other ($n = 2$). Sporadic prion disease cases ($n = 23$) included probable cases ($n = 10$) and autopsy-confirmed definite cases ($n = 13$, of subtypes: 6 MM1, 3 VV2 and 4 other/unknown). Genetic prion disease cases ($n = 11$) included D178N ($n = 2$), E200K ($n = 7$), and V210I ($n = 2$). After receipt in our lab, samples were thawed, spiked with 0.03% CHAPS detergent (final concentration) and stored in 30 μl aliquots for mass spectrometry analysis. Sample handling histories before receipt in our lab are not well-documented and are likely variable because of the large number of referring physicians sending these samples to surveillance centers, but systematic differences between diagnostic groups are unlikely because all samples were similarly referred for diagnostic testing on suspicion of prion disease.

Samples were de-identified and broken into five batches (to be run on different days) randomly using an R script. Assay operators were blinded to diagnosis. The methods and values obtained for PrP

[1] The abbreviations used are: PrP, prion protein; AAA, amino acid analysis; CSF, cerebrospinal fluid; MRM, multiple reaction monitoring.

ELISA, hemoglobin, and total protein measurements on these CSF samples were previously reported (3).

Rat and cynomolgus monkey CSF were purchased from BioIVT. Human brain tissue was from a nonprion disease control individual provided by the National Prion Disease Pathology Surveillance Center (Cleveland, OH). Mouse brain tissue from Edinburgh PrP knockout mice (30) backcrossed to a C57BL/10 background (31), and matching tissue from wild-type C57BL/10 mice, were provided by Gregory J. Raymond (NIAID Rocky Mountain Labs, Hamilton, MT).

Recombinant Prion Protein Preparation and Isotopic Labeling—Untagged recombinant HuPrP23–230 (MW = 22,878) and MoPrP23–231 (MW = 23,151), corresponding to full-length post-translationally modified human and mouse PrP without the signal peptide or GPI signal but retaining an N-terminal methionine, were purified by denaturation and Ni-NTA affinity from *E. coli* inclusion bodies as previously described (32, 33), using a vector generously provided by Byron Caughey (NIAID Rocky Mountain Labs, Hamilton, MT). ^{15}N incorporation was achieved by growing the *E. coli* in ^{15}N cell growth medium (Cambridge Isotope Laboratories CGM-1000-N) induced with ^{15}N auto-induction medium (Millipore 71759–3). Purified protein was formulated in 0.03% CHAPS and aliquoted in single-use tubes to avoid repetitive freeze/thaw cycles. Protein concentration was determined by amino acid analysis (AAA, New England Peptide). Percent ^{15}N isotopic incorporation was estimated using LC-MS/MS. ^{15}N labeled human recombinant prion protein (10 μg) was digested and desalted following the procedure as described in *PrP MRM assay* and analyzed as described in *Pilot LC-MS/MS analysis*. Precursor masses for ^{15}N were extracted from the chromatograms using XCalibur software Qualbrowser software (Thermo) 3.0.63 with a 6 *m/z* window of centered on the precursors and charge states listed in supplemental Table S1. Isotopic envelopes between protein expressed in ^{15}N-containing media and standard media were compared visually. Summation of all observed m/z peak areas less than the ^{12}C monoisotopic mass peak were compared with summation of all expected isotope peak to estimate the overall completeness of ^{15}N incorporation (supplemental Fig. S1).

LC-MS/MS Analyses of CSF and Recombinant PrP—Samples of dried digested recombinant proteins or human cerebrospinal fluid (processed as described in *PrP MRM assay*) were reconstituted in 3% acetonitrile/5% acetic acid to a final concentration of ~1 μg total protein per 1 μl and analyzed in a single injection using a standard 2 h reversed-phase gradient. LC-MS/MS was performed using a QExactive mass spectrometer (Thermo) equipped with a Proxeon Easy-nLC 1200 and a custom built nanospray source (James A. Hill Instrument Services). Samples were injected (1 to 2 μg) onto a 75 μm ID PicoFrit column (New Objective) packed to 20 cm with Reprosil-Pur C18 AQ 1.9 μm media (Dr. Maisch) and heated to 50 °C. MS source conditions were set as follows: spray voltage 2000, capillary temperature 250, S-lens RF level 50. A single Orbitrap MS scan from 300 to 1800 *m/z* at a resolution of 70,000 with AGC set at 3e6 was followed by up to 12 MS/MS scans at a resolution of 17,500 with AGC set at 5e4. MS/MS spectra were collected with normalized collision energy of 25 and isolation width of 2.5 amu. Dynamic exclusion was set to 20 s and peptide match was set to preferred. Mobile phases consisted of 3% acetonitrile/0.1% formic acid as solvent A, 90% acetonitrile/0.1% formic acid as solvent B. Flow rate was set to 200 nL/min throughout the gradient, 2–6% B in 1 min, 6–30% B in 84 min, 30–60% B in 9 min, 60–90% B in 1 min with a hold at 90% B for 5 min. MS data were analyzed using Spectrum Mill MS Proteomics Workbench software Rev B.06.01.202 (Agilent Technologies). Similar MS/MS spectra acquired on the same precursor *m/z* within ± 60 s were merged. MS/MS spectra were excluded from searching if they failed the quality filter by not having a sequence tag length > 0 (*i.e.* minimum of two masses separated by the in-chain mass of an amino acid) or did not have a precursor MH+ in the range of 600–6000. All extracted spectra were searched against a UniProt database containing human and mouse reference proteome sequences (UniProt.human.mouse.20141017.RNFISnr.150contams, *n* = 100,236 entries) downloaded from the UniProt web site on October 17, 2014 with redundant sequences removed. A set of common laboratory contaminant proteins (150 sequences) were appended to this database and verified to contain the sequences for human and mouse major prion protein. The database was searched with the following parameters. ESI-QEXACTIVE-HCD-v2 scoring, parent and fragment mass tolerance of 20 ppm, 40% minimum matched peak intensity and 'trypsin' enzyme specificity up to 2 missed cleavages. Fixed modification was carbamidomethylation at cysteine and variable modifications were oxidized methionine, deamidation of asparagine and pyro-glutamic acid. Database matches were autovalidated at the peptide and protein level in a two-step process with optimized scores & R1-R2 score thresholds with maximum false discovery rate (FDR) of 1.2% across each LC run by target-decoy-based searches using reversed sequences. The list of identified proteins was further filtered to contain proteins and protein isoforms with at least 2 unique peptides and an aggregate protein score greater than 20. Protein-peptide comparison report comprised of all validated peptides was exported which included a ranked summary by intensity of all peptides unique to prion protein. Hits were ranked by total summed MS1 intensity of all identified peptides for each protein (totalIntensitySpecies column). Summary data are available as a supplementary Excel file or in the online GitHub repository for this study (see Data Availability).

Selection of PrP Peptides for MRM Assay Development—Nine peptides covering 4 species were selected from computational and empirical data (supplemental Table S2 and supplemental Figs. S2–S4). PrP amino acid sequences (supplemental Fig. S4) were obtained from UniProt (34) and aligned using Clustal O 1.2.4 (35). Peptides were prioritized based our criteria previously described (36, 37) as outlined and described in detail in supplemental Fig. S2. Peptides were checked for uniqueness to human PrP using the Peptide String Match utility in Spectrum Mill (http://proteomics.broadinstitute.org). Peptides were selected based on PrP biology and desired assay applications described in Results (Fig. 1). One peptide, PIIHFGSDYEDR, was included after being detected in CSF despite an N-terminal proline.

All nine peptides were synthesized (New England Peptide) using stable isotope labeled [$^{15}N_4{}^{13}C_6$]Arg or [$^{15}N_2{}^{13}C_6$]Lys at the C terminus and purified peptide specifications previously outlined (>95% chemical purity, >99% isotopic purity, quantified by AAA) to qualify as standards for Tier 1 or 2 assays (27). Mixtures of all 9 heavy peptides were formulated in 30% acetonitrile/0.1% formic acid and aliquotted into single-use tubes to avoid freeze thaw throughout the study. Before each set of samples, 50 fmol was injected and analyzed using the same LC-MRM-MS method used for samples to confirm LC column and MS performance.

System Suitability Standards—An equimolar predigested "Bovine 6 Protein Mix" (PTD/00001/63) was purchased from Bruker-Michrom, Inc. Pierce™ Peptide Retention Time Calibration Mixture (88320) was purchased from Thermo. Both dried peptide standard mixtures were resuspended in 3% acetonitrile/5% acetic and 50 fmol were injected and analyzed by LC-MRM-MS at the beginning, the middle and at the end of each set of samples and visually inspected in a Skyline document to confirm LC column and MS performance. Transitions for Bovine protein mix and PRTC are provided in supplemental Tables S1*B* and S1*C* respectively.

PrP MRM Assay—In devising a CSF sample preparation protocol, we drew upon our experience with MRM analysis of plasma (38) and published mass spectrometry protocols for prion studies (39, 40). Except where otherwise specified, all samples contained 0.03% CHAPS, a zwitterionic detergent, because this reduces preanalytical

loss of PrP because of plastic adsorption (3). The elution conditions of the desalting step (see below) were designed to reduce the amount of CHAPS in the sample before LC-MS. Unlike many other detergents, CHAPS impact on chromatography and peptide ionization is minimized because it elutes off C18 later in the reversed-phase gradient (>60% acetonitrile).

^{15}N Protein Standard Addition For Human Samples—For human CSF clinical samples, endogenous PrP was quantified relative to uniformly labeled ^{15}N-labeled recombinant HuPrP23–230 (starting concentration 2.42 mg/ml determined by AAA) with an estimated isotopic incorporation >97.5% (see Recombinant Protein Preparation) diluted 1:5000 in phosphate-buffered saline containing 1 mg/ml bovine serum albumin and 0.03% CHAPS. This solution was then further diluted 1:20 (1.5 μl added into 30 μl) into CSF samples (final concentration 24.2 ng/ml) before the denaturation and digestion workflow described below. ELISA analysis indicated that this concentration of carrier protein and detergent was enough to keep recombinant PrP in solution and avoid loss to plastic, without appreciably affecting CSF total protein content.

Sample Digestion—All concentrations listed below are final concentrations. For each replicate, 30 μl of CSF with 0.03% CHAPS was incubated with 6 M urea (Sigma U0631) and 20 mM TCEP (Pierce 77720) at 37 °C while shaking at 800 rpm in an Eppendorf Thermomixer for 30 min to denature the protein and reduce disulfide bonds. 39 mM iodoacetamide was added for 30 min in the dark at room temperature to alkylate cysteine residues. Urea was diluted to 900 mM by the addition of 0.2 Trizma pH 8.1 (Sigma T8568) to permit trypsin activity. One microgram of trypsin (Promega V5113) was added (final concentration of ~1.4 ng/μl), providing at least a 1:50 trypsin:substrate ratio for CSF samples with total protein content <1.6 mg/ml, which includes 97% of CSF samples we have analyzed (3). Trypsin digestion proceeded overnight shaking at 800 rpm at 37 °C. Digestion was stopped with 5% formic acid and samples were transferred to 4 °C until desalt. To permit quantification of PrP in preclinical species samples, a mix containing 100 fmol of each ^{15}N/^{13}C-labeled synthetic heavy peptide was then added to the CSF digests (3.33 nM peptide, equivalent to ~76 ng/ml full-length PrP based on an approximate molecular weight of 22.8 kDa). Digestion was quenched by 5% formic acid and samples were kept at 4 °C until desalt.

Synthetic Peptide Addition For Multi-species Assay—To permit quantification of PrP in preclinical species samples, a mix containing 100 fmol of each ^{15}N/^{13}C-labeled synthetic heavy peptide (3.33 nM peptide, equivalent to ~76 ng/ml full-length PrP based on an approximate molecular weight of 22.8 kDa) was added after digest and before sample desalt. Other aspects of the procedure described above and below were unchanged.

Sample Desalt—To desalt the samples, StageTips (41) comprised of two punches of C18 material (Empore 66883-U) fitted into a 200 μl pipette tip using a 16 gauge needle with 90° blunt ends (Cadence Science 7938) and a PEEK tubing puncher (Idex 1567) were placed onto microcentrifuge tubes using an adapter (Glycen CEN.24). Tubes were centrifuged at 2500 × *g* for 3 min after each step, as follows: conditioning with 50 μl 90% acetonitrile/0.1% trifluoroacetic acid; equilibration with 50 μl 0.1% trifluoroacetic acid and priming with 10 μl 0.1% trifluoroacetic acid (no spin after priming); addition of CSF digest in increments of 150 μl; two washes with 50 μl of 0.1% trifluoroacetic acid; and two elutions into a new microcentrifuge tube with 50 μl of 40% acetonitrile/0.1% trifluoroacetic acid. Eluates were frozen at −80 °C.

LC-MRM-MS Analysis—Frozen samples were dried under vacuum centrifugation and resuspended in 12 μl 3% acetonitrile/5% acetic acid and placed into a vortexer for 5 min at room temperature. Samples were then centrifuged at 12,000 × *g* for 5 min and 10 μl of the supernatant was transferred to an HPLC vial (Waters 186000273). HPLC vials were centrifuged briefly (30–60 s) at 1200 × *g* to remove air bubbles and transferred into the nanoLC autosampler compartment set to 7 °C. Samples were analyzed on a TSQ Quantiva triple quadrupole mass spectrometer installed with a Nanospray Flex source and Easy-nLC 1000 system (Thermo). Ion source was set to positive ion mode with capillary temperature of 300 °C, spray voltage of 2000 and sweep gas set to 0. The Easy-nLC 1000 system was primed with mobile phase A (3% acetonitrile/0.1% formic acid), mobile phase B (90% acetonitrile/0.1% formic acid). Samples were injected (2 μl, 20% of digested sample) onto a 0.075 mm ID PicoFrit (New Objective) column pulled to a 10 μm emitter and custom-packed to 20 cm with 1.9 μm 200Å C18-AQ Reprosil beads (Dr. Maisch). The LC gradient was 0% B to 30% B for 55 min, 30% B to 60% B in 5 min, 60% B to 90% B in 1 min using a flow rate of 200 nL/min. Collision energies were optimized over 4 steps, 2.5 V per step in batches of less than 500 transitions per batch. Three to four transitions were monitored per peptide using the MRM transitions listed in supplemental Table S1 using a 1.5 s cycle time. In addition, even though the corresponding heavy peptides were not synthesized, we monitored for the transitions that corresponded to the oxidized methionine version of the peptide VVEQMCITQYER.

Data Analysis—Extracted Ion chromatograms (XIC) of all transition ions were verified and integrated using a Skyline document as described (42) (Skyline version 4.1.0.11796, https://brendanx-uw1.gs.washington.edu/labkey/project/home/software/Skyline/begin.view) that contained the sequences and spectral libraries derived from LC-MS/MS of the ^{15}N/^{13}C-labeled synthetic heavy peptides. After peak integration, the Skyline report file was exported as a text delimited file where the peak areas in the columns labeled as "Light," "Heavy," or "15N" for the single most intense, interference-free, reproducibly measured transition (supplemental Table S1) were used for quantification and subsequent statistical analysis. Interferences were identified by manual inspection of XICs between light and heavy peptides. Light or heavy transitions with different relative intensity ratios compared with standards or had asymmetric peaks were excluded from further analysis. Columns included for export were: Protein Name, Protein Gene, Protein Species, Peptide Sequence, Peptide Modified Sequence, File Name, Acquired Time, Replicate Name, SampleGroup, Peptide Retention Time, Precursor *m/z*, Fragment Ion, Area, Area Ratio, Total Area, Total Area Ratio.

To determine the response of each peptide in terms of L:^{15}N ratio as well as evaluate dilution linearity of the assay, we spiked 0, 2.4, 24, or 240 ng/ml of ^{15}N-labeled recombinant human PrP into a single control CSF sample (from an individual with normal pressure hydrocephalus) in triplicate. For each peptide, we then fitted a linear model correlating the (nonzero) spiked concentrations to the observed ^{15}N: light ratios with the intercept fixed at zero, yielding slopes ranging from 39 to 448 ng/ml. Each peptide was then assigned a response factor equal to the highest slope observed for any peptide (448 ng/ml) divided by its own slope. This response factor was multiplied by the L:^{15}N ratio for each peptide in each sample to obtain a normalized estimate of protein concentration.

In $n = 12$ individual replicates (out of 110) of the clinical samples, the oxidized methionine (met-ox) version of the VVEQMCITQYER peptide was more abundant than the reduced version, despite the inclusion of a reduction step in sample preparation. The VVEQMCITQYER peptide was omitted from analysis for these replicates.

RESULTS

Design of the PrP MRM Assay—PrP ranked number 8 in intensity out of 322 confidently detected proteins in single-shot, LC-MS/MS analysis of human CSF digested with trypsin (see Methods). This indicated that PrP was a good candidate

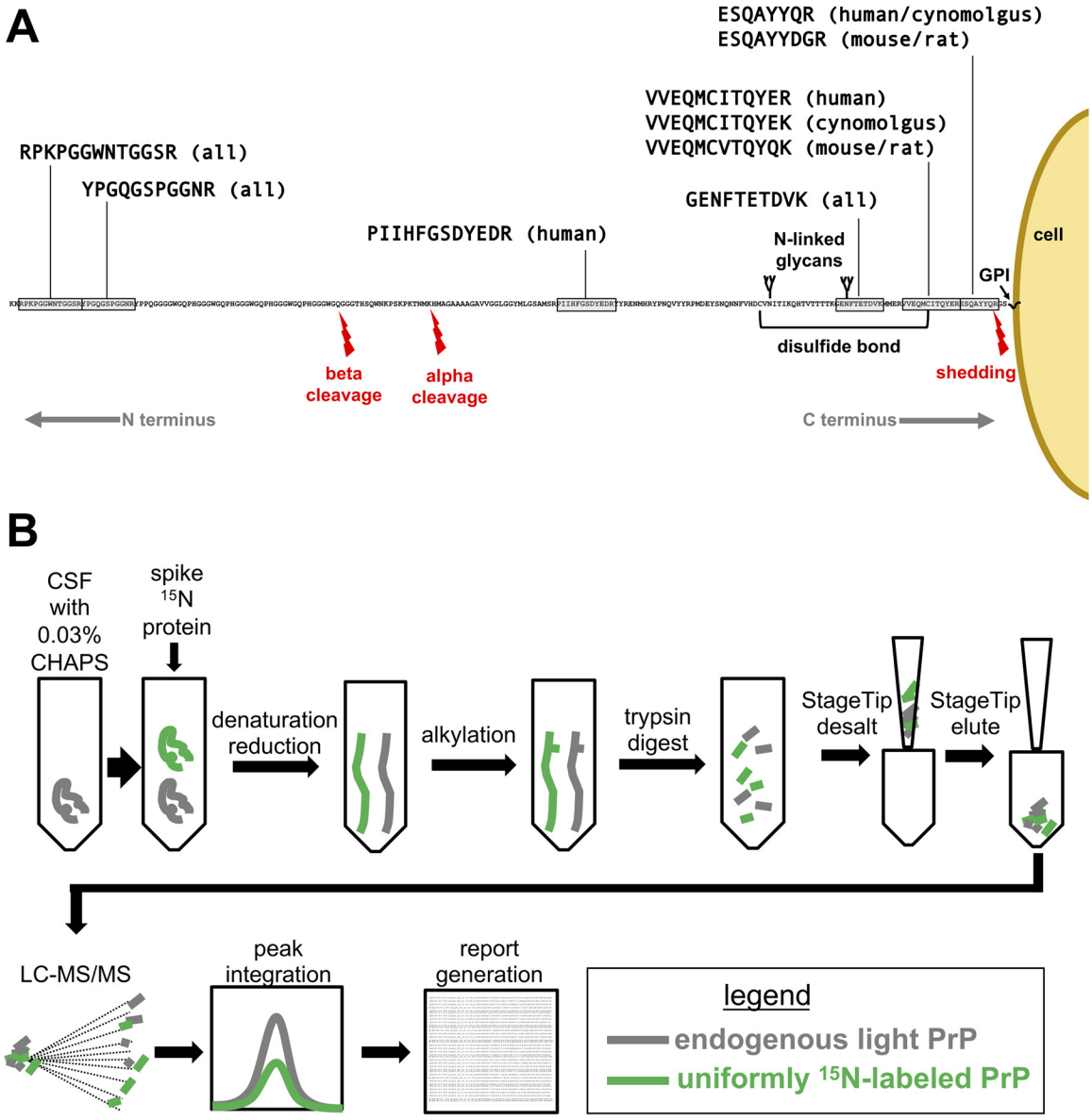

FIG. 1. **Design of the PrP MRM assay.** *A*, Selection of PrP tryptic peptides for MRM. The full sequence of human PrP (residues 23–230) after post-translational modifications (removal of signal peptide residues 1–22 and GPI signal residues 231–253) is shown, GPI-anchored to the outer leaflet of the plasma membrane, with the position of selected peptides and their rodent or monkey orthologs shown relative to the positions of N-linked glycans, a disulfide bond, and endogenous proteolytic events (8). *B*, PrP MRM workflow as described in Methods.

for direct analysis by LC-MRM-MS in CSF without additional fractionation (43) or enrichment methods (44). PrP peptides with the highest MS intensities after digestion of recombinant human or mouse PrP as well as human CSF were preferentially ranked according to criteria described in Methods and supplemental Fig. S2. We selected six human peptides, as well as three orthologous peptides specific to mouse, rat, and/or cynomolgus macaque PrP, to support assay application to preclinical drug development (Fig. 1*A*, supplemental Fig. S4, and supplemental Table S2). Peptides were chosen to span the N- and C-terminal domains of PrP, up- and downstream of alpha and beta cleavage sites, allowing us to quantify proteolytic fragments of cleaved PrP (Fig. 1*A* and supplemental Fig. S4).

We further designed a workflow for the PrP MRM assay (Fig. 1*B*) incorporating an incubation in the presence of a strong chaotrope to denature both properly folded and misfolded forms of PrP. We then reduced and alkylated the protein mixture to break the disulfide bonds and prevent them from refolding, and thereby make the whole protein accessible to the enzymatic processing of r-trypsin. To permit quantification of endogenous unlabeled (hereafter "light") PrP, we added uniformly ^{15}N-labeled recombinant human PrP (hereafter "^{15}N") into clinical samples before analysis (Fig. 1*B*).

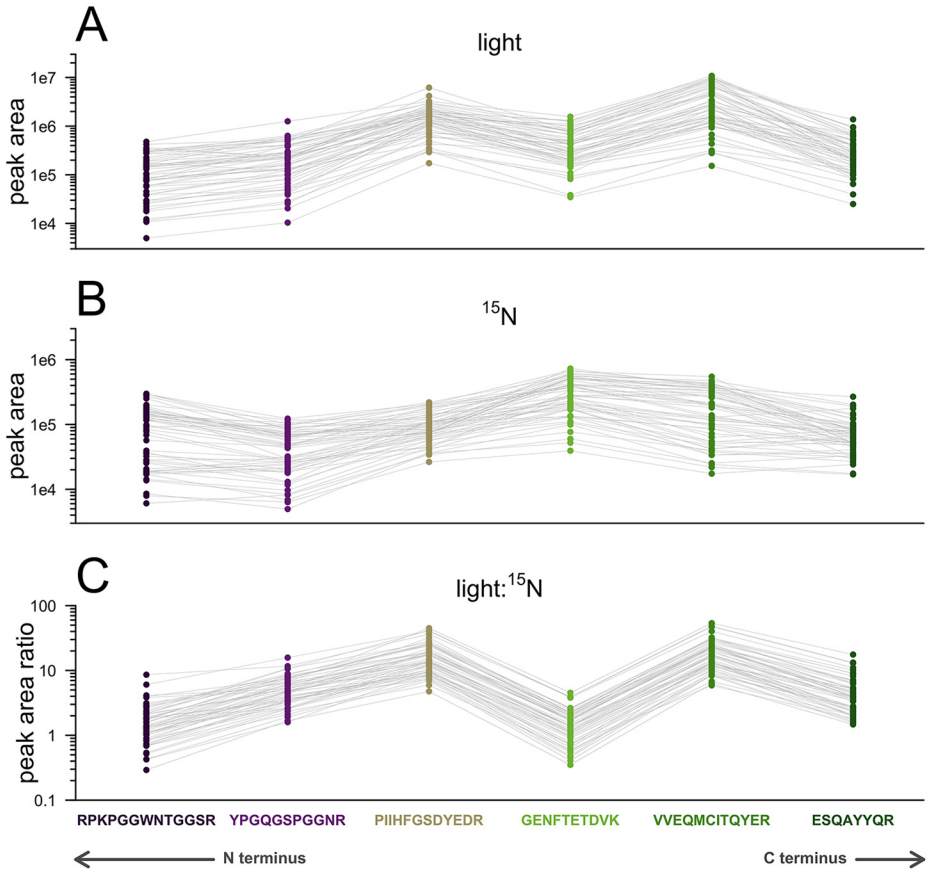

FIG. 2. **Relative recovery of six human PrP peptides in CSF.** For each of $n = 55$ clinical samples, panels show each peptide's *A*, light peak area, *B*, ^{15}N peak area, and *C*, light:^{15}N ratio. Gray lines connect the dots representing distinct peptides from the same individual. Peak area ratios shown here are not normalized by peptide response factors, and so reflect differences in recovery between peptides.

Compared with synthetic heavy peptides, the use of an isotopically labeled full-length protein standard controls for analytical variability that can occur during enzymatic digestion and solid phase extraction (SPE) using StageTips (41), and can, in principle, provide a more accurate quantitative measure of the amount of each of the peptides derived from the target protein (38, 45).

Assessment of Human PrP Assay Performance—To support measurement of endogenous unlabeled PrP in $n = 55$ human CSF clinical samples (see next section), we performed quality control analysis using the ^{15}N protein added into each sample. Clinical samples were divided into 5 batches run on separate days; each sample was processed in duplicate on the same day, stored at −80 °C, and later analyzed in duplicate, also on the same day. A common control sample was also measured in duplicate on each day.

The mean absolute MS response, either from ^{15}N recombinant or from endogenous light PrP, varied by over an order of magnitude between the six PrP peptides (Fig. 2*A*–2*B*). The recovery of the six peptides from endogenous PrP relative to one another was preserved across CSF patient samples (Fig. 2*A*), but differed from the recovery of the corresponding peptides derived from ^{15}N recombinant PrP (Fig. 2*B*), resulting in a ~10-fold difference in mean light:^{15}N ratio between different peptides (Fig. 2*C* and supplemental Table S3), which was consistent across days (supplemental Fig. S5). Such differences in response are expected and may reflect differences in both digestion efficiencies under the urea/trypsin conditions used here (46) and electrospray ionization efficiencies (43, 47, 48) of these peptides.

Another factor driving the difference in response between peptides may be the post-translational modification (Fig. 1*A*) of endogenous PrP in CSF relative to the bacterially expressed recombinant ^{15}N version used as reference. For example, a significant proportion of brain PrP is N-terminally truncated (12), and PrP cleavage products have been observed in CSF as well (11). PrP is known to be variably glycosylated at residue N197, but our assay will only detect the nonglycosylated form of the GENFTETDVK peptide containing this site. This may account for the much lower response of this peptide in CSF *versus* the ^{15}N standard (Fig. 2). For the C-terminal peptide ESQAYYQR, our assay might not detect proteolytically shed PrP if the cut site for ADAM10, the predominant PrP sheddase (49), in human PrP is homologous to its reported cut site in rodent PrP (9, 50). For the most N-terminal peptide monitored, RPKPGGWNTGGSR, we detected a retained N-terminal methionine three residues upstream of this sequence in bacterially expressed PrP (supplemental Fig. S3), consistent with reported N-terminal methionine excision patterns in *E. coli* (51). This could alter this peptide's trypsin digest efficiency relative to brain and CSF PrP. Because we lacked access to purified full-length mammalian PrP to serve

TABLE I

Performance reproducibility of six human peptides in human CSF samples. Mean intra-day CV (based on same-day process duplicates of n = 55 samples); mean inter-day CV (based on a single inter-day control CSF sample analyzed in duplicate on n = 5 separate days; and inter-individual CV among the 55 different samples

Codons	Peptide	Mean intra-day assay CV	Mean inter-day assay CV	Inter-individual CV
25–37	RPKPGGWNTGGSR	10%	16%	80%
38–48	YPGQGSPGGNR	12%	22%	52%
137–148	PIIHFGSDYEDR	10%	12%	56%
195–204	GENFTETDVK	9%	12%	58%
209–220	VVEQMCITQYER	9%	12%	54%
221–228	ESQAYYQR	10%	18%	70%

a reference standard, we cannot definitively dissect the reasons for the differences in recovery between peptides. Accordingly, we assigned each peptide a response factor based on the slope of the light:^{15}N ratio observed in the ^{15}N dose-response experiment (Methods, supplemental Fig. S6). Multiplying the raw light:^{15}N ratios by these peptide-specific response factors brought each peptide's abundance into line with the highest-responding peptide, and yielded normalized estimates of CSF PrP concentration in CSF that averaged 421 ng/ml across samples and all peptides (supplemental Table S3, supplemental Fig. S6).

All six peptides exhibited strong technical performance on par with previously published MRM assays (38, 43, 44, 47). Mean same-day process replicate CVs were below 15% both overall (Table I) and within each quartile across the range of low- to high-PrP samples (supplemental Table S4). Inter-day process replicate CVs were below 25%. Although PrP MRM is currently a Tier 2 assay, this intra-day and inter-day reproducibility would be consistent with Tier 1 assay requirements as described for targeted MS-based peptide measurement fit-for-purpose and is also within the best practice guidelines for clinical MRM assays (27, 52, 53). We did not formally determine lower and upper limits of quantification, but we observed response linearity across a dilution series of high- and low-PrP human CSF samples (supplemental Fig. S5) and over two orders of magnitude with spiked ^{15}N recombinant human PrP (supplemental Fig. S6) as surrogate analyte across the range of expected PrP concentrations in clinical samples.

These data suggest that PrP MRM is suitable for estimating the amount of PrP in CSF and measuring changes in abundance within and between patients. In further support of the applicability of this multiplex assay to answering biological questions in clinical samples, we found that for every peptide, the variability in amount of PrP between patient samples was much larger than the analytical variability, with inter-individual CVs of 52–80% contrasting with the observed tight process replicate agreement of ~10% CV (Table I). Given that analytical variability was much smaller than biological variability, all six peptides were deemed suitable for analysis in clinical samples, and, owing to their different positions within PrP's amino acid sequence (Fig. 1*A*), each peptide was deemed able to inform independently upon the presence of its particular protein domain in CSF.

PrP Peptide Abundance Is Reduced in the CSF of Patients With Prion Disease—We used PrP MRM to quantify CSF PrP peptides in $n = 55$ clinical samples from individuals with rapidly progressive dementia referred to prion surveillance centers for testing and who ultimately either received nonprion disease diagnoses, or in whom sporadic or genetic prion disease was confirmed by autopsy (see Methods). All six human PrP peptides quantified by PrP MRM showed a marked decrease in abundance in prion disease patients compared with nonprion diagnoses, and all six peptides showed the same general pattern, with nonprion disease patients' CSF samples giving the highest mean peptide level, followed by sporadic prion disease, followed by genetic prion disease (Fig. 3*A*). The results from MRM mirrored the previously reported PrP ELISA results for these same 55 individuals (3) (Fig. 3*B*), but differed in the estimated absolute amounts of PrP by ~3-fold.

Relationship Between PrP MRM and ELISA—Across the clinical samples, each peptide's abundance was positively correlated to the full-length PrP concentration determined by ELISA (Fig. 4*A*). The coefficients of correlation, from 0.40 to 0.72, are within the ranges reported for other MRM assays compared with corresponding immunoassays (44, 47, 54). All peptides were strongly correlated to one another, with coefficients of correlation ranging from 0.67 to 0.96, and no obvious differences within *versus* between protein domains (N- and C-terminal; Fig. 4*B*). The linear relationships between peptides were preserved across the range of samples analyzed (supplemental Fig. S5). These results, together with the fact that the magnitude of decrease in abundance in prion disease cases was similar for all peptides (Fig. 4*A*), suggested that PrP MRM and ELISA may be measuring the same analyte — predominantly full-length PrP. We therefore asked whether PrP MRM could serve as an orthogonal method to validate findings recently reported for ELISA.

Because plastic adsorption is reported to cause substantial loss of PrP in preanalytical handling, and detergent is reported to largely mitigate this (3), we analyzed replicates of one CSF sample by MRM with and without 0.03% CHAPS detergent. As with ELISA, we found that the addition of CHAPS increased PrP peptide recovery by an average of 51% (p = 2.3e-8, Type I ANOVA). (The clinical CSF samples and recom-

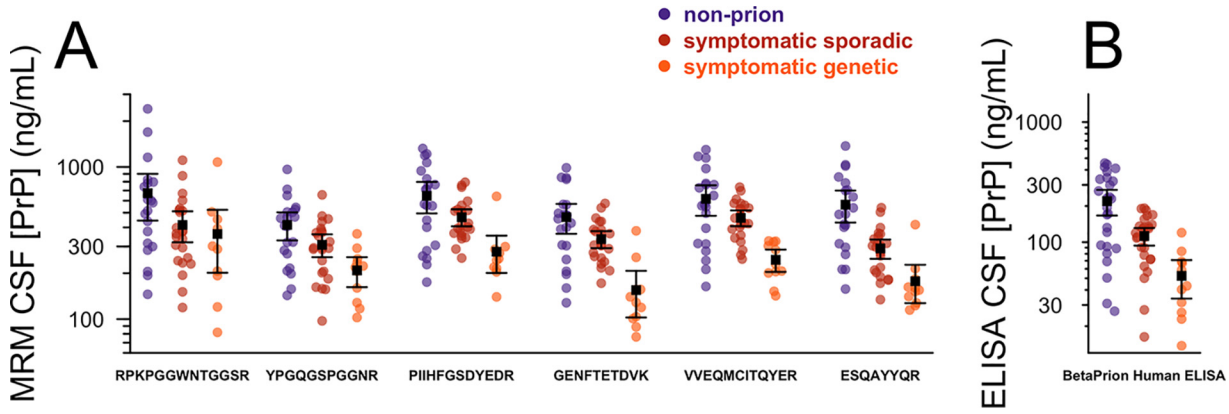

FIG. 3. **Relative abundance of PrP as measured by six independent peptides is decreased in the CSF of prion disease patients.** *CSF PrP* concentrations in $n = 55$ clinical CSF samples determined by *A*, PrP MRM for each of six peptides, normalized by peptide response factors to obtain PrP concentrations in ng/ml and arranged with the most N-terminal peptide at left and the most C-terminal peptide at right, compared with *B*, previously reported PrP ELISA results for the same samples, reproduced from Vallabh et al. (3). Black squares and bars show the mean and 95% confidence interval of the mean for each group.

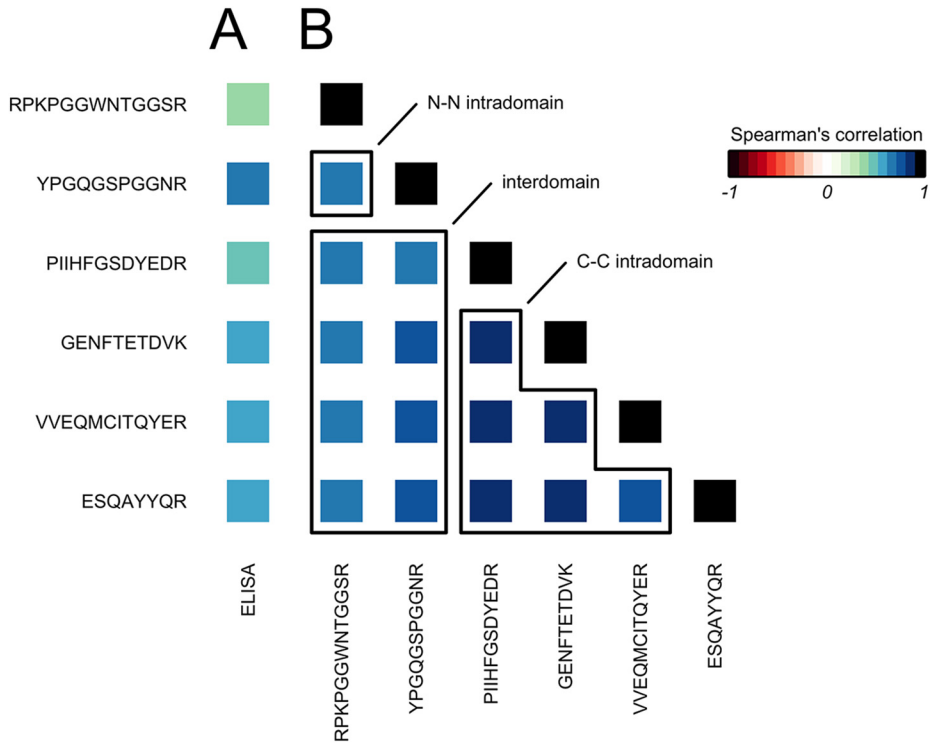

FIG. 4. **Correlations among PrP MRM peptides and with ELISA.** *A*, Spearman's correlation between each peptide measured in MRM versus total PrP by ELISA. *B*, Spearman's correlation between every combination of peptides measured in MRM. All $p < 0.01$.

binant protein used in this study contained added 0.03% CHAPS, see Methods).

To compare PrP MRM and ELISA results while introducing covariates, we calculated a final estimated PrP concentration from MRM for each CSF sample by averaging the normalized PrP concentration across the six peptides. The estimated PrP concentrations obtained by MRM and by ELISA were correlated across CSF samples ($r = 0.61$, Spearman's correlation, $p = 1.3e\text{-}6$). MRM PrP concentration was uncorrelated with CSF hemoglobin ($p = 0.85$, Spearman's correlation), supporting the conclusion that blood contamination is not a source of CSF PrP (3).

The concentration of PrP in CSF measured by ELISA is correlated with the total protein concentration in CSF (3). This might reflect a true biological correlation across individuals, or it could reflect pre-analytical factors, if other proteins in CSF serve a blocking function, mitigating PrP loss to plastic during sample handling (3). A potential concern, however, is that such a correlation could also arise if other proteins found in the human CSF also nonspecifically bind in the ELISA and contribute to background signal. If true, this would call into question the ability of ELISA-based PrP measurement to accurately measure a specific drug-dependent or disease state-dependent decrease in PrP concentration. To distinguish be-

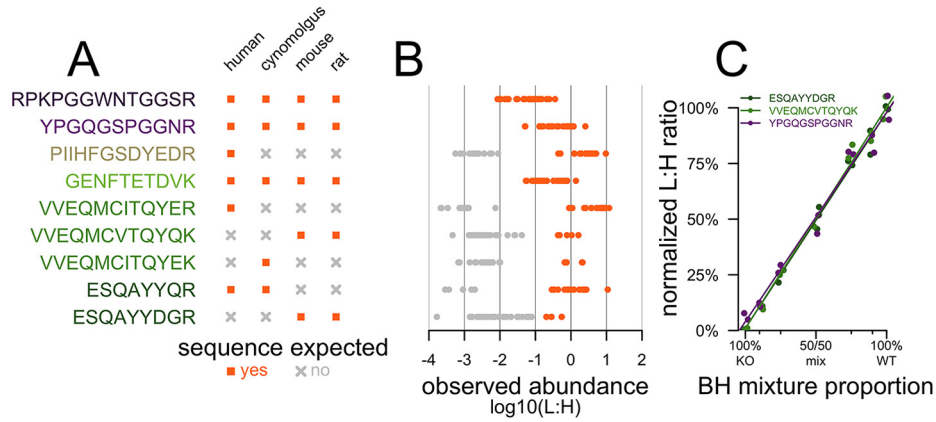

FIG. 5. **Development of the PrP MRM assay for preclinical species of interest.** *A*, Control chart of the species expected for the peptides selected for this study, $n = 6$ human, $n = 5$ monkey, $n = 5$ mouse, and $n = 5$ rat. *B*, Sensitivity and selectivity across species. Data from $n = 19$ samples ($n = 4$ cynomolgous macaque CSF, $n = 10$ human CSF, $n = 1$ mouse brain, and $n = 4$ rat CSF) in a total of $n = 35$ replicates were analyzed. L:H peptide ratios are shown for peptides expected in the respective species' samples (sequence-matched, orange) versus not expected (nonmatched, gray). All species-specific peptides were observed in the sequence-matched species at least an order of magnitude above the noise observed in nonsequence-matched species, except for ESQAYYDGR (sequence-matched species: mouse, rat), for which the separation was only about half an order of magnitude. *C*, 10% brain homogenate from wild-type mice (WT) or Edinburgh PrP knockout mice (30) (KO) were mixed in seven different proportions (all KO, 10/90, 25/75, 50/50, 75/25, 90/10, and all WT), further diluted to 0.5% brain homogenate in saline and 0.03% CHAPS, and assayed by PrP MRM. Of the five peptides sequence-matched to mouse PrP, the three with best performance in this experiment (mean process replicate CV <10%) are shown here, again with individual replicates jittered along the x axis so that separate points are visible. Each peptide's L:H ratio is normalized to the average value of the two "all WT" replicates, and best-fit lines are shown. All three peptides exhibit good linearity, with y-intercepts very close to zero, as expected for PrP knockout mice, and adjusted R^2 values ranging 98.2% - 99.0% (linear regression).

tween these possible explanations for the reported PrP-total protein correlation, we tested the relationships between ELISA PrP concentration, MRM PrP concentration, and total protein concentration among our clinical samples. The correlation between ELISA PrP concentration and total protein concentration was marginal but observable among the 55 samples analyzed here (+94 ng/ml PrP per 1 mg total protein, $p = 0.043$, linear regression: ELISA PrP ~ total protein), but this relationship vanished completely when MRM PrP concentration was included as a covariate ($p = 0.60$ for total protein in linear regression: ELISA PrP ~ MRM PrP + total protein). Likewise, MRM PrP concentration was itself correlated to total protein (+238 ng/ml PrP per 1 mg/ml total protein, $p = 0.017$, linear regression: MRM PrP ~ total protein). Together, the observations that the relationship between PrP and total protein was replicated in MRM, and that total protein did not explain any residual variance in ELISA-measured PrP after controlling for MRM-measured PrP, suggest that the correlation between CSF PrP and total protein in CSF is a genuine property of the samples analyzed, and that ELISA is specifically measuring PrP in human CSF.

Application of PrP MRM to Preclinical Species of Interest—Because the existing ELISA assay is specific to human PrP (3), we sought to apply PrP MRM to analysis of tissues from species of interest for preclinical drug development. Synthetic peptides can offer advantages over full-length recombinant proteins for the development of targeted MS assays: they are quicker and less expensive to generate and quantify, and can be multiplexed to measure a number of proteins simultaneously. To test this for PrP and construct species-specific MRM assays, we quantified endogenous "light" PrP relative to $^{15}N/^{13}C$ single residue labeled ("heavy") synthetic peptides that were spiked after trypsin digestion to quantify mouse, rat, or monkey PrP (supplemental Fig. S7). To assess cross-species selectivity and sensitivity, we analyzed human, rat, and cynomolgus macaque CSF as well as mouse and human brain homogenate, and compared observed results to the expected presence or absence of each peptide for each species based on amino acid sequence (Fig. 5*A*). For the six PrP peptides harboring sequence differences between species (Fig. 1*A*, supplemental Table S2), we observed slight differences in the retention time, best transition ion, and/or response level (supplemental Table S1, supplemental Table S5). We also found the MRM assay to be highly selective when the MS response between species for these peptides was compared. Each peptide consistently detected in sequence-matched species above the background level observed in nonsequence-matched species (Fig. 5*B*). Process replicate mean coefficients of variation (CVs) were <15% for all peptides, in line with our previous experience (38) suggesting that heavy peptide standards can provide precision on par with full-length recombinant protein, albeit with different recovery levels (supplemental Table S5). We found that the total protein and lipid content of brain tissue complicated analysis of ≥1% w/v brain homogenates, but 0.5% w/v brain homogenates proved technically tractable in PrP MRM. Using mixtures of wild-type mouse brain homoge-

nates titrated into a background of PrP knockout mouse brain homogenate, we confirmed a linear response for three mouse sequence-matched peptides, demonstrating the specificity of the assay for lowered PrP within a complex brain-derived peptide mixture (Fig. 5*C*).

DISCUSSION

Here we describe a targeted mass spectrometry assay for measuring CSF PrP. Six of six human PrP peptides we quantified, from the N to the C terminus, were lowered in prion disease patients compared with nonprion disease patients. CSF PrP may therefore be difficult to interpret as a pharmacodynamic biomarker in symptomatic prion disease patients, because the direct effect of a PrP-lowering drug and the effect of disease process alleviation would be expected to push CSF PrP in opposing directions. Instead, trials to demonstrate target engagement and perform dose-finding for a PrP-lowering drug will likely need to be conducted in presymptomatic individuals at risk for genetic prion disease (3, 6). Preliminary evidence suggests that test-retest stability of CSF PrP in individuals without active prion disease is good (CV $<$ 13%), and a clinical research study to validate this finding in at-risk PrP mutation carriers is underway (3, 55). If CSF PrP, absent drug treatment, is indeed stable over time in presymptomatic mutation carriers, then a drug-dependent decrease of 40%, as recently observed for mutant huntingtin in an antisense oligonucleotide trial (56), should be readily quantifiable.

Our data support the interpretability of CSF PrP in such a trial context, for three reasons. First, we provide evidence that CSF PrP is a simple, well-behaved analyte: all PrP peptides behave similarly. This contrasts with the complex situation reported for tau isoforms in CSF (57, 58), and suggests that various approaches to measuring PrP in CSF can all be interpreted to reflect the level of the relevant, disease-causing protein. Second, we confirm that CSF PrP is not correlated with CSF hemoglobin. This supports the brain and not blood origin of CSF PrP and leads us to expect that pharmacologic lowering of brain PrP will be mirrored in CSF. Third, we replicate the reported (3) correlation between CSF PrP and CSF total protein content. The correlation between PrP and total protein might reflect genuine biological variables such as age and CSF flow rate (59), and/or it might arise from preanalytical variables (3), but our observation of this correlation by both mass spectrometry and ELISA argues against the possibility that this correlation simply results from matrix interference in ELISA. This finding supports the overall interpretability of findings from prior, ELISA-based, studies of CSF PrP.

Our study has several limitations. First, we have only compared samples between prion and nonprion disease patients to examine the effect of the disease state on CSF PrP. Determining the effect of PrP-lowering drug treatment on CSF PrP is a priority for future work. Second, we still cannot exclude the possibility that protein misfolding contributes somewhat to the decrease in CSF PrP that we observe, because the chaotrope used here—6 M urea—has not been proven to denature all misfolded PrP. This concentration of urea was shown to abolish 99.99% of hamster prion infectivity (60), but prion strains differ in their conformational stability (25). Human prions unfold at ~3 M guanidine hydrochloride (61–63), but urea is a less potent denaturant (64). Third, because bacterially expressed recombinant PrP is an imperfect standard by which to quantify mammalian PrP, our data do not support any firm conclusions about the baseline composition of PrP in terms of different cleavage products in human CSF generally. A ^{15}N protein standard purified from a mammalian expression system would better account for the digestion efficiencies of PrP in CSF. Nevertheless, by comparing the abundance of each PrP peptide between diagnostic categories — individuals with and without prion disease — we do establish that any changes driven by the disease state apparently affect all domains of PrP equally. This finding is not inconsistent with existing literature: for example, the PrP C2 fragment resulting from beta cleavage is known to be increased in brain parenchyma during prion disease (26), but if C2 is then retained in intracellular aggregates rather than being shed, whereas its counterpart N2 is rapidly degraded, then increased beta cleavage might result in both N- and C-terminal PrP peptides being decreased in prion disease CSF, as observed here.

The specificity for PrP peptides observed across species and in wild-type *versus* PrP knockout mouse brain suggests that PrP MRM should be useful in preclinical development of PrP-lowering drugs. PrP MRM is currently a Tier 2 targeted assay (27), with partial analytical validation suggesting a potential for further work to elevate it to Tier 1 and enable clinical use. Given the likely important role of CSF PrP as a biomarker in future prion disease therapeutic development, and the different pros and cons of ELISA and MRM methods, availability of both assays will be an asset. For clinical measurements of a single protein, wider instrument availability sometimes favors the use of ELISA, but there are counter-examples, such as thyroglobulin, where patients' anti-idiotypic antibodies can lead to false ELISA readings (65). Targeted MS measurements avoid such interference, because any autoantibodies are reduced to peptides before analysis. In addition, PrP MRM may offer other advantages over ELISA, including the use of a single assay across preclinical animals and clinical studies as well as wide dynamic range without sample dilution. Finally, because PrP MRM monitors well-defined peptide analytes, any potential for interference from post-translational modifications or patient missense mutations can be determined *a priori* based on sequence information. Adaptation of PrP MRM for clinical use will require modifications and improvements to the protocol described here. The LC/MS gradient of 45 min we used is longer than the 5–10 min expected for high-throughput clinical biomarker assays. To transition to clinical use, feasibility and performance should be assessed

at a faster gradient under higher (*e.g.* microflow) conditions using commercially available C18 columns. An increase in assay throughput may come at the cost of some sensitivity, but because all PrP peptides in this study demonstrated comparable behavior across this set of clinical samples, a future implementation of PrP MRM might choose to monitor fewer or even a single peptide, facilitating the implementation of a significantly faster assay. In addition, we ported assay parameters that we use for plasma-based MRM (38, 43) without extensive optimization. Thus, testing and improvement of digest and cleanup conditions could further improve recovery and performance. Finally, once such an assay is implemented, robust bioanalytical method validation will be expected if the assay is to be used in clinical decision-making (38, 43, 66, 67).

Our data and methods provide a proof of concept for MRM-based quantification of PrP in CSF and provide a roadmap for further development of the assay for eventual use in the clinic.

DATA AVAILABILITY

All processed data and source code for this study are provided in a public GitHub repository at https://github.com/ericminikel/prp_mrm and are sufficient to reproduce the analyses and figures herein. This repository also includes a summary table for download containing the MRM results (light and ^{15}N peak areas, light:^{15}N ratio and normalized PrP concentration in ng/mL) for all clinical samples and all peptides. Skyline files have been uploaded to Panorama (68) at https://panoramaweb.org/yVRdi1.url and data can be downloaded from ProteomeXchange (http://proteomecentral.proteomexchange.org/cgi/GetDataset?ID=PXD014781).

* This study was supported by the Next Generation Fund at the Broad Institute, BroadIgnite, the National Institutes of Health (F31 AI122592 to E.V.M.), the National Science Foundation (GRFP 2015214731 to S.M.V.), individual philanthropic donations to the Broad Institute and to Prion Alliance, and an anonymous organization. Sample collection in Göttingen was supported by Bundesministerium für Gesundheit (grant 1369-341) through Robert Koch Institute. This work was also supported in part by grants from the National Cancer Institute (NCI) Clinical Proteomic Tumor Analysis Consortium (NIH/NCI U24-CA210986 and NIH/NCI U01 CA214125 to S.A.C.). The content is solely the responsibility of the authors and does not necessarily represent the official views of the National Institutes of Health. The authors declare that they have no conflicts of interest with the contents of this article.

[S] This article contains supplemental material.

§§§§ These authors contributed equally to this work.

‡‡‡‡ To whom correspondence may be addressed. Tel.: 617 714 7000; E-mail: minikel@broadinstitute.org.

¶¶¶¶ To whom correspondence may be addressed. Tel.: 617 714 7000; E-mail: scarr@broad.mit.edu.

Author contributions: E.V.M., E.K., S.M.V., M.D.M., R.O., S.L.S., and S.A.C. designed research; E.V.M., E.K., A.R.C., S.M.V., C.R.H., and A.G.R. performed research; E.V.M., E.K., and A.R.C. analyzed data; E.V.M., E.K., and S.A.C. wrote the paper; J.G.S., G.J.R., F.L., I.Z., S.C., and P.P. contributed new reagents/analytic tools.

REFERENCES

1. Prusiner, S. B. (1998) Prions. *Proc. Natl. Acad. Sci. U.S.A.* **95,** 13363–13383
2. Raymond, G. J., Zhao, H. T., Race, B., Raymond, L. D., Williams, K., Swayze, E. E., Graffam, S., Le, J., Caron, T., Stathopoulos, J., O'Keefe, R., Lubke, L. L., Reidenbach, A. G., Kraus, A., Schreiber, S. L., Mazur, C., Cabin, D. E., Carroll, J. B., Minikel, E. V., Kordasiewicz, H., Caughey, B., and Vallabh, S. M. (2019) Antisense oligonucleotides extend survival of prion-infected mice. *JCI Insight* **5,** pii: 131175
3. Vallabh, S. M., Nobuhara, C. K., Llorens, F., Zerr, I., Parchi, P., Capellari, S., Kuhn, E., Klickstein, J., Safar, J. G., Nery, F. C., Swoboda, K. J., Geschwind, M. D., Zetterberg, H., Arnold, S. E., Minikel, E. V., and Schreiber, S. L. (2019) Prion protein quantification in human cerebrospinal fluid as a tool for prion disease drug development. *Proc. Natl. Acad. Sci.*, **116,** 7793–7798
4. Minikel, E. V., Vallabh, S. M., Lek, M., Estrada, K., Samocha, K. E., Sathirapongsasuti, J. F., McLean, C. Y., Tung, J. Y., Yu, L. P. C., Gambetti, P., Blevins, J., Zhang, S., Cohen, Y., Chen, W., Yamada, M., Hamaguchi, T., Sanjo, N., Mizusawa, H., Nakamura, Y., Kitamoto, T., Collins, S. J., Boyd, A., Will, R. G., Knight, R., Ponto, C., Zerr, I., Kraus, T. F. J., Eigenbrod, S., Giese, A., Calero, M., de Pedro-Cuesta, J., Haïk, S., Laplanche, J.-L., Bouaziz-Amar, E., Brandel, J.-P., Capellari, S., Parchi, P., Poleggi, A., Ladogana, A., O'Donnell-Luria, A. H., Karczewski, K. J., Marshall, J. L., Boehnke, M., Laakso, M., Mohlke, K. L., Kähler, A., Chambert, K., McCarroll, S., Sullivan, P. F., Hultman, C. M., Purcell, S. M., Sklar, P., van der Lee, S. J., Rozemuller, A., Jansen, C., Hofman, A., Kraaij, R., van Rooij, J. G. J., Ikram, M. A., Uitterlinden, A. G., van Duijn, C. M., Exome Aggregation Consortium (ExAC), Daly, M. J., and MacArthur, D. G. (2016) Quantifying prion disease penetrance using large population control cohorts. *Sci. Transl. Med.* **8,** 322ra9
5. Minikel, E. V., Vallabh, S. M., Orseth, M. C., Brandel, J.-P., Haïk, S., Laplanche, J.-L., Zerr, I., Parchi, P., Capellari, S., Safar, J., Kenny, J., Fong, J. C., Takada, L. T., Ponto, C., Hermann, P., Knipper, T., Stehmann, C., Kitamoto, T., Ae, R., Hamaguchi, T., Sanjo, N., Tsukamoto, T., Mizusawa, H., Collins, S. J., Chiesa, R., Roiter, I., de Pedro-Cuesta, J., Calero, M., Geschwind, M. D., Yamada, M., Nakamura, Y., and Mead, S. (2019) Age at onset in genetic prion disease and the design of preventive clinical trials. *Neurology* **93,** e125–e134
6. Vallabh, S. M. (2019) *Antisense oligonucleotides for the prevention of genetic prion disease.* PhD dissertation, Harvard University, Cambridge, MA
7. Food, U. S., Drug Administration . (2017) Critical Path Innovation Meeting: Genetic Prion Disease. November 14, 2017. Requestor: Broad Institute.
8. Altmeppen, H. C., Puig, B., Dohler, F., Thurm, D. K., Falker, C., Krasemann, S., and Glatzel, M. (2012) Proteolytic processing of the prion protein in health and disease. *Am. J. Neurodegener. Dis.* **1,** 15–31
9. Linsenmeier, L., Mohammadi, B., Wetzel, S., Puig, B., Jackson, W. S., Hartmann, A., Uchiyama, K., Sakaguchi, S., Endres, K., Tatzelt, J., Saftig, P., Glatzel, M., and Altmeppen, H. C. (2018) Structural and mechanistic aspects influencing the ADAM10-mediated shedding of the prion protein. *Mol. Neurodegener.* **13,** 18
10. Tagliavini, F., Prelli, F., Porro, M., Salmona, M., Bugiani, O., and Frangione, B. (1992) A soluble form of prion protein in human cerebrospinal fluid: implications for prion-related encephalopathies. *Biochem. Biophys. Res. Commun.* **184,** 1398–1404
11. Schmitz, M., Schlomm, M., Hasan, B., Beekes, M., Mitrova, E., Korth, C., Breil, A., Carimalo, J., Gawinecka, J., Varges, D., and Zerr, I. (2010) Codon 129 polymorphism and the E200K mutation do not affect the cellular prion protein isoform composition in the cerebrospinal fluid from patients with Creutzfeldt-Jakob disease. *Eur. J. Neurosci.* **31,** 2024–2031
12. Chen, S. G., Teplow, D. B., Parchi, P., Teller, J. K., Gambetti, P., and Autilio-Gambetti, L. (1995) Truncated forms of the human prion protein in normal brain and in prion diseases. *J. Biol. Chem.* **270,** 19173–19180
13. Fevrier, B., Vilette, D., Archer, F., Loew, D., Faigle, W., Vidal, M., Laude, H., and Raposo, G. (2004) Cells release prions in association with exosomes. *Proc. Natl. Acad. Sci. U.S.A.* **101,** 9683–9688
14. Meyne, F., Gloeckner, S. F., Ciesielczyk, B., Heinemann, U., Krasnianski, A., Meissner, B., and Zerr, I. (2009) Total prion protein levels in the cerebrospinal fluid are reduced in patients with various neurological disorders. *J. Alzheimers Dis.* **17,** 863–873
15. Dorey, A., Tholance, Y., Vighetto, A., Perret-Liaudet, A., Lachman, I., Krolak-Salmon, P., Wagner, U., Struyfs, H., De Deyn, P. P., El-Moualij, B.,

Zorzi, W., Meyronet, D., Streichenberger, N., Engelborghs, S., Kovacs, G. G., and Quadrio, I. (2015) Association of cerebrospinal fluid prion protein levels and the distinction between Alzheimer disease and Creutzfeldt-Jakob disease. *JAMA Neurol.* **72,** 267–275
16. Abu Rumeileh, S., Lattanzio, F., Stanzani Maserati, M., Rizzi, R., Capellari, S., and Parchi, P. (2017) Diagnostic Accuracy of a Combined Analysis of Cerebrospinal Fluid t-PrP, t-tau, p-tau, and Aβ42 in the Differential Diagnosis of Creutzfeldt-Jakob Disease from Alzheimer's Disease with Emphasis on Atypical Disease Variants. *J. Alzheimers Dis.* **55,** 1471–1480
17. Villar-Piqué, A., Schmitz, M., Lachmann, I., Karch, A., Calero, O., Stehmann, C., Sarros, S., Ladogana, A., Poleggi, A., Santana, I., Ferrer, I., Mitrova, E., Žáková, Pocchiari, D. M., Baldeiras, I., Calero, M., Collins, S. J., Geschwind, M. D., Sánchez-Valle, R., Zerr, I., and Llorens, F. (2018) Cerebrospinal fluid total prion protein in the spectrum of prion diseases. *Mol. Neurobiol.* **56,** 2811–2821
18. Schulz-Schaeffer, W. J., Tschöke, S., Kranefuss, N., Dröse, W., Hause-Reitner, D., Giese, A., Groschup, M. H., and Kretzschmar, H. A. (2000) The paraffin-embedded tissue blot detects PrP(Sc) early in the incubation time in prion diseases. *Am. J. Pathol.* **156,** 51–56
19. Safar, J. G., DeArmond, S. J., Kociuba, K., Deering, C., Didorenko, S., Bouzamondo-Bernstein, E., Prusiner, S. B., and Tremblay, P. (2005) Prion clearance in bigenic mice. *J. Gen. Virol.* **86,** 2913–2923
20. Moreno, J. A., Radford, H., Peretti, D., Steinert, J. R., Verity, N., Martin, M. G., Halliday, M., Morgan, J., Dinsdale, D., Ortori, C. A., Barrett, D. A., Tsaytler, P., Bertolotti, A., Willis, A. E., Bushell, M., and Mallucci, G. R. (2012) Sustained translational repression by eIF2α-P mediates prion neurodegeneration. *Nature* **485,** 507–511
21. Parchi, P., Giese, A., Capellari, S., Brown, P., Schulz-Schaeffer, W., Windl, O., Zerr, I., Budka, H., Kopp, N., Piccardo, P., Poser, S., Rojiani, A., Streichemberger, N., Julien, J., Vital, C., Ghetti, B., Gambetti, P., and Kretzschmar, H. (1999) Classification of sporadic Creutzfeldt-Jakob disease based on molecular and phenotypic analysis of 300 subjects. *Ann. Neurol.* **46,** 224–233
22. Caughey, B., Raymond, G. J., Ernst, D., and Race, R. E. (1991) N-terminal truncation of the scrapie-associated form of PrP by lysosomal protease(s): implications regarding the site of conversion of PrP to the protease-resistant state. *J. Virol.* **65,** 6597–6603
23. Goold, R., McKinnon, C., Rabbanian, S., Collinge, J., Schiavo, G., and Tabrizi, S. J. (2013) Alternative fates of newly formed PrPSc upon prion conversion on the plasma membrane. *J. Cell Sci.* **126,** 3552–3562
24. Mays, C. E., Kim, C., Haldiman, T., van der Merwe, J., Lau, A., Yang, J., Grams, J., Di Bari, M. A., Nonno, R., Telling, G. C., Kong, Q., Langeveld, J., McKenzie, D., Westaway, D., and Safar, J. G. (2014) Prion disease tempo determined by host-dependent substrate reduction. *J. Clin. Invest.* **124,** 847–858
25. Safar, J., Wille, H., Itri, V., Groth, D., Serban, H., Torchia, M., Cohen, F. E., and Prusiner, S. B. (1998) Eight prion strains have PrP(Sc) molecules with different conformations. *Nat. Med.* **4,** 1157–1165
26. Watts, J. C., Stöhr, J., Bhardwaj, S., Wille, H., Oehler, A., Dearmond, S. J., Giles, K., and Prusiner, S. B. (2011) Protease-resistant prions selectively decrease Shadoo protein. *PLoS Pathog.* **7,** e1002382
27. Carr, S. A., Abbatiello, S. E., Ackermann, B. L., Borchers, C., Domon, B., Deutsch, E. W., Grant, R. P., Hoofnagle, A. N., Hüttenhain, R., Koomen, J. M., Liebler, D. C., Liu, T., MacLean, B., Mani, D. R., Mansfield, E., Neubert, H., Paulovich, A. G., Reiter, L., Vitek, O., Aebersold, R., Anderson, L., Bethem, R., Blonder, J., Boja, E., Botelho, J., Boyne, M., Bradshaw, R. A., Burlingame, A. L., Chan, D., Keshishian, H., Kuhn, E., Kinsinger, C., Lee, J. S. H., Lee, S.-W., Moritz, R., Oses-Prieto, J., Rifai, N., Ritchie, J., Rodriguez, H., Srinivas, P. R., Townsend, R. R., Van Eyk, J., Whiteley, G., Wiita, A., and Weintraub, S. (2014) Targeted peptide measurements in biology and medicine: best practices for mass spectrometry-based assay development using a fit-for-purpose approach. *Mol. Cell. Proteomics* **13,** 907–917
28. Hermann, P., Laux, M., Glatzel, M., Matschke, J., Knipper, T., Goebel, S., Treig, J., Schulz-Schaeffer, W., Cramm, M., Schmitz, M., and Zerr, I. (2018) Validation and utilization of amended diagnostic criteria in Creutzfeldt-Jakob disease surveillance. *Neurology* **91,** e331–e338
29. Orrú, C. D., Groveman, B. R., Hughson, A. G., Zanusso, G., Coulthart, M. B., and Caughey, B. (2015) Rapid and sensitive RT-QuIC detection of human Creutzfeldt-Jakob disease using cerebrospinal fluid. *mBio* **6,** pii: e02451-14
30. Manson, J. C., Clarke, A. R., Hooper, M. L., Aitchison, L., McConnell, I., and Hope, J. (1994) 129/Ola mice carrying a null mutation in PrP that abolishes mRNA production are developmentally normal. *Mol. Neurobiol.* **8,** 121–127
31. Striebel, J. F., Race, B., Pathmajeyan, M., Rangel, A., and Chesebro, B. (2013) Lack of influence of prion protein gene expression on kainate-induced seizures in mice: studies using congenic, coisogenic and transgenic strains. *Neuroscience* **238,** 11–18
32. Wilham, J. M., Orrú, C. D., Bessen, R. A., Atarashi, R., Sano, K., Race, B., Meade-White, K. D., Taubner, L. M., Timmes, A., and Caughey, B. (2010) Rapid end-point quantitation of prion seeding activity with sensitivity comparable to bioassays. *PLoS Pathog.* **6,** e1001217
33. Orrù, C. D., Groveman, B. R., Hughson, A. G., Manca, M., Raymond, L. D., Raymond, G. J., Campbell, K. J., Anson, K. J., Kraus, A., and Caughey, B. (2017) RT-QuIC assays for prion disease detection and diagnostics. *Methods Mol. Biol.* **1658,** 185–203
34. The UniProt Consortium (2017) UniProt: the universal protein knowledgebase. *Nucleic Acids Res.* **45,** D158–D169
35. Sievers, F., and Higgins, D. G. (2018) Clustal Omega for making accurate alignments of many protein sequences. *Protein Sci. Publ. Protein Soc.* **27,** 135–145
36. Kuhn, E., and Carr, S. A. (2016) Multiplexed immunoaffinity enrichment of peptides with anti-peptide antibodies and quantification by stable isotope dilution multiple reaction monitoring mass spectrometry. *Methods Mol. Biol.* **1410,** 135–167
37. Hoofnagle, A. N., Whiteaker, J. R., Carr, S. A., Kuhn, E., Liu, T., Massoni, S. A., Thomas, S. N., Townsend, R. R., Zimmerman, L. J., Boja, E., Chen, J., Crimmins, D. L., Davies, S. R., Gao, Y., Hiltke, T. R., Ketchum, K. A., Kinsinger, C. R., Mesri, M., Meyer, M. R., Qian, W.-J., Schoenherr, R. M., Scott, M. G., Shi, T., Whiteley, G. R., Wrobel, J. A., Wu, C., Ackermann, B. L., Aebersold, R., Barnidge, D. R., Bunk, D. M., Clarke, N., Fishman, J. B., Grant, R. P., Kusebauch, U., Kushnir, M. M., Lowenthal, M. S., Moritz, R. L., Neubert, H., Patterson, S. D., Rockwood, A. L., Rogers, J., Singh, R. J., Van Eyk, J. E., Wong, S. H., Zhang, S., Chan, D. W., Chen, X., Ellis, M. J., Liebler, D. C., Rodland, K. D., Rodriguez, H., Smith, R. D., Zhang, Z., Zhang, H., and Paulovich, A. G. (2016) Recommendations for the generation, quantification, storage, and handling of peptides used for mass spectrometry-based assays. *Clin. Chem.* **62,** 48–69
38. Kuhn, E., Whiteaker, J. R., Mani, D. R., Jackson, A. M., Zhao, L., Pope, M. E., Smith, D., Rivera, K. D., Anderson, N. L., Skates, S. J., Pearson, T. W., Paulovich, A. G., and Carr, S. A. (2012) Interlaboratory evaluation of automated, multiplexed peptide immunoaffinity enrichment coupled to multiple reaction monitoring mass spectrometry for quantifying proteins in plasma. *Mol. Cell. Proteomics* **11,** M111.013854
39. Moore, R. A., Head, M. W., Ironside, J. W., Ritchie, D. L., Zanusso, G., Choi, Y. P., Pyo Choi, Y., and Priola, S. A. (2016) The distribution of prion protein allotypes differs between sporadic and iatrogenic Creutzfeldt-Jakob disease patients. *PLoS Pathog.* **12,** e1005416
40. Moore, R. A., Ward, A., Race, B., and Priola, S. A. (2018) Processing of high-titer prions for mass spectrometry inactivates prion infectivity. *Biochim. Biophys. Acta Proteins Proteomics* **1866,** 1174–1180
41. Rappsilber, J., Mann, M., and Ishihama, Y. (2007) Protocol for micro-purification, enrichment, pre-fractionation and storage of peptides for proteomics using StageTips. *Nat. Protoc.* **2,** 1896–1906
42. Broudy, D., Killeen, T., Choi, M., Shulman, N., Mani, D. R., Abbatiello, S. E., Mani, D., Ahmad, R., Sahu, A. K., Schilling, B., Tamura, K., Boss, Y., Sharma, V., Gibson, B. W., Carr, S. A., Vitek, O., MacCoss, M. J., and MacLean, B. (2014) A framework for installable external tools in Skyline. *Bioinforma. Oxf. Engl.* **30,** 2521–2523
43. Keshishian, H., Addona, T., Burgess, M., Kuhn, E., and Carr, S. A. (2007) Quantitative, multiplexed assays for low abundance proteins in plasma by targeted mass spectrometry and stable isotope dilution. *Mol. Cell. Proteomics* **6,** 2212–2229
44. Kuhn, E., Addona, T., Keshishian, H., Burgess, M., Mani, D. R., Lee, R. T., Sabatine, M. S., Gerszten, R. E., and Carr, S. A. (2009) Developing multiplexed assays for troponin I and interleukin-33 in plasma by peptide immunoaffinity enrichment and targeted mass spectrometry. *Clin. Chem.* **55,** 1108–1117
45. Abbatiello, S. E., Schilling, B., Mani, D. R., Zimmerman, L. J., Hall, S. C., MacLean, B., Albertolle, M., Allen, S., Burgess, M., Cusack, M. P., Gosh, M., Hedrick, V., Held, J. M., Inerowicz, H. D., Jackson, A., Keshishian, H.,

Kinsinger, C. R., Lyssand, J., Makowski, L., Mesri, M., Rodriguez, H., Rudnick, P., Sadowski, P., Sedransk, N., Shaddox, K., Skates, S. J., Kuhn, E., Smith, D., Whiteaker, J. R., Whitwell, C., Zhang, S., Borchers, C. H., Fisher, S. J., Gibson, B. W., Liebler, D. C., MacCoss, M. J., Neubert, T. A., Paulovich, A. G., Regnier, F. E., Tempst, P., and Carr, S. A. (2015) Large-scale interlaboratory study to develop, analytically validate and apply highly multiplexed, quantitative peptide assays to measure cancer-relevant proteins in plasma. *Mol. Cell. Proteomics* **14,** 2357–2374

46. Scott, K. B., Turko, I. V., and Phinney, K. W. (2015) Quantitative performance of internal standard platforms for absolute protein quantification using multiple reaction monitoring-mass spectrometry. *Anal. Chem.* **87,** 4429–4435
47. Keshishian, H., Addona, T., Burgess, M., Mani, D. R., Shi, X., Kuhn, E., Sabatine, M. S., Gerszten, R. E., and Carr, S. A. (2009) Quantification of cardiovascular biomarkers in patient plasma by targeted mass spectrometry and stable isotope dilution. *Mol. Cell. Proteomics* **8,** 2339–2349
48. Fusaro, V. A., Mani, D. R., Mesirov, J. P., and Carr, S. A. (2009) Prediction of high-responding peptides for targeted protein assays by mass spectrometry. *Nat. Biotechnol.* **27,** 190–198
49. Altmeppen, H. C., Prox, J., Puig, B., Kluth, M. A., Bernreuther, C., Thurm, D., Jorissen, E., Petrowitz, B., Bartsch, U., De Strooper, B., Saftig, P., and Glatzel, M. (2011) Lack of a-disintegrin-and-metalloproteinase ADAM10 leads to intracellular accumulation and loss of shedding of the cellular prion protein in vivo. *Mol. Neurodegener.* **6,** 36
50. Taylor, D. R., Parkin, E. T., Cocklin, S. L., Ault, J. R., Ashcroft, A. E., Turner, A. J., and Hooper, N. M. (2009) Role of ADAMs in the ectodomain shedding and conformational conversion of the prion protein. *J. Biol. Chem.* **284,** 22590–22600
51. Frottin, F., Martinez, A., Peynot, P., Mitra, S., Holz, R. C., Giglione, C., and Meinnel, T. (2006) The proteomics of N-terminal methionine cleavage. *Mol. Cell. Proteomics* **5,** 2336–2349
52. Lee, J. W., Devanarayan, V., Barrett, Y. C., Weiner, R., Allinson, J., Fountain, S., Keller, S., Weinryb, I., Green, M., Duan, L., Rogers, J. A., Millham, R., O'Brien, P. J., Sailstad, J., Khan, M., Ray, C., and Wagner, J. A. (2006) Fit-for-purpose method development and validation for successful biomarker measurement. *Pharm. Res.* **23,** 312–328
53. Grant, R. P., and Hoofnagle, A. N. (2014) From lost in translation to paradise found: enabling protein biomarker method transfer by mass spectrometry. *Clin. Chem.* **60,** 941–944
54. Kuhn, E., Wu, J., Karl, J., Liao, H., Zolg, W., and Guild, B. (2004) Quantification of C-reactive protein in the serum of patients with rheumatoid arthritis using multiple reaction monitoring mass spectrometry and 13C-labeled peptide standards. *Proteomics* **4,** 1175–1186
55. Vallabh, S. (2017) Prion Alliance sponsors MGH research study. *PrionAlliance.org*
56. Tabrizi, S. J., Leavitt, B. R., Landwehrmeyer, G. B., Wild, E. J., Saft, C., Barker, R. A., Blair, N. F., Craufurd, D., Priller, J., Rickards, H., Rosser, A., Kordasiewicz, H. B., Czech, C., Swayze, E. E., Norris, D. A., Baumann, T., Gerlach, I., Schobel, S. A., Paz, E., Smith, A. V., Bennett, C. F., and Lane, R. M. (2019) Targeting huntingtin expression in patients with Huntington's disease. *N. Engl. J. Med.* **380,** 2307–2316
57. Meredith, J. E., Sankaranarayanan, S., Guss, V., Lanzetti, A. J., Berisha, F., Neely, R. J., Slemmon, J. R., Portelius, E., Zetterberg, H., Blennow, K., Soares, H., Ahlijanian, M., and Albright, C. F. (2013) Characterization of novel CSF Tau and ptau biomarkers for Alzheimer's disease. *PloS One* **8,** e76523
58. Sato, C., Barthélemy, N. R., Mawuenyega, K. G., Patterson, B. W., Gordon, B. A., Jockel-Balsarotti, J., Sullivan, M., Crisp, M. J., Kasten, T., Kirmess, K. M., Kanaan, N. M., Yarasheski, K. E., Baker-Nigh, A., Benzinger, T. L. S., Miller, T. M., Karch, C. M., and Bateman, R. J. (2018) Tau kinetics in neurons and the human central nervous system. *Neuron* **97,** 1284–1298.e7
59. McCudden, C. R., Brooks, J., Figurado, P., and Bourque, P. R. (2017) Cerebrospinal fluid total protein reference intervals derived from 20 years of patient data. *Clin. Chem.* **63,** 1856–1865
60. Prusiner, S. B., Groth, D., Serban, A., Stahl, N., and Gabizon, R. (1993) Attempts to restore scrapie prion infectivity after exposure to protein denaturants. *Proc. Natl. Acad. Sci. U.S.A.* **90,** 2793–2797
61. Kim, C., Haldiman, T., Cohen, Y., Chen, W., Blevins, J., Sy, M.-S., Cohen, M., and Safar, J. G. (2011) Protease-sensitive conformers in broad spectrum of distinct PrPSc structures in sporadic Creutzfeldt-Jakob disease are indicator of progression rate. *PLoS Pathog.* **7,** e1002242
62. Kim, C., Haldiman, T., Surewicz, K., Cohen, Y., Chen, W., Blevins, J., Sy, M.-S., Cohen, M., Kong, Q., Telling, G. C., Surewicz, W. K., and Safar, J. G. (2012) Small protease sensitive oligomers of PrPSc in distinct human prions determine conversion rate of PrP(C). *PLoS Pathog.* **8,** e1002835
63. Cescatti, M., Saverioni, D., Capellari, S., Tagliavini, F., Kitamoto, T., Ironside, J., Giese, A., and Parchi, P. (2016) Analysis of conformational stability of abnormal prion protein aggregates across the spectrum of Creutzfeldt-Jakob disease prions. *J. Virol.* **90,** 6244–6254
64. Greene, R. F., and Pace, C. N. (1974) Urea and guanidine hydrochloride denaturation of ribonuclease, lysozyme, alpha-chymotrypsin, and beta-lactoglobulin. *J. Biol. Chem.* **249,** 5388–5393
65. Hoofnagle, A. N., and Wener, M. H. (2006) Serum thyroglobulin: a model of immunoassay imperfection. *Clin Lab Int* **8,** 12–14
66. Whiteaker, J. R., Halusa, G. N., Hoofnagle, A. N., Sharma, V., MacLean, B., Yan, P., Wrobel, J. A., Kennedy, J., Mani, D. R., Zimmerman, L. J., Meyer, M. R., Mesri, M., Rodriguez, H., Clinical Proteomic Tumor Analysis Consortium (CPTAC), Paulovich, A. G. (2014) CPTAC Assay Portal: a repository of targeted proteomic assays. *Nat. Methods* **11,** 703–704
67. Food and Drug Administration (2018) Bioanalytical Method Validation. Guidance for Industry.
68. Sharma, V., Eckels, J., Schilling, B., Ludwig, C., Jaffe, J. D., MacCoss, M. J., and MacLean, B. (2018) Panorama public: a public repository for quantitative data sets processed in Skyline. *Mol. Cell. Proteomics MCP* **17,** 1239–1244

SUPPLEMENTAL DATA

Domain-specific quantification of prion protein in cerebrospinal fluid by targeted mass spectrometry

Eric Vallabh Minikel[1,2,3,†,*], Eric Kuhn[4,*], Alexandra R Cocco[4], Sonia M Vallabh[1,2,3], Christina R Hartigan[4], Andrew G Reidenbach[1], Jiri G Safar[5], Gregory J Raymond[6], Michael D McCarthy[7], Rhonda O'Keefe[7], Franc Llorens[8,9], Inga Zerr[8], Sabina Capellari[10,11], Piero Parchi[10,12], Stuart L Schreiber[1,13], Steven A Carr[4,†]

Supplemental Tables

Table S1A. Precursor and product characteristics for all PrP peptides monitored. *Best fragment ions were chosen as transition ions with the highest peak area that were also interference-free and reproducibly measured in pilot studies.*

peptide modified sequence	precursor charge	fragment ion	product charge	precursor mz [light]	precursor mz [heavy]	precursor mz [$_{15}$N]	product mz [light]	product mz [heavy]	product mz [15n]	best fragment ion
PIIHFGSDYEDR	3	b4	1	483.57	486.90	489.21	461.29	461.29	467.27	
	3	y9	2	483.57	486.90	489.21	563.23	568.24	570.21	
	3	y4	1	483.57	486.90	489.21	582.25	592.26	589.23	y4
	3	y7	1	483.57	486.90	489.21	841.33	851.34	851.30	
RPKPGGWNTGGSR	3	y4	1	457.24	460.58	464.55	376.19	386.20	383.17	y4
	3	y5	1	457.24	460.58	464.55	477.24	487.25	485.22	
	3	y6	1	457.24	460.58	464.55	591.28	601.29	601.25	
YPGQGSPGGNR	2	y5	1	545.26	550.26	553.23	500.26	510.27	509.23	y5
	2	y7	1	545.26	550.26	553.23	644.31	654.32	655.28	
	2	y9	1	545.26	550.26	553.23	829.39	839.40	843.35	
GENFTETDVK	2	y4	1	570.26	574.27	576.25	462.26	470.27	467.24	
	2	y5	1	570.26	574.27	576.25	591.30	599.31	597.28	
	2	y6	1	570.26	574.27	576.25	692.35	700.36	699.33	
	2	y7	1	570.26	574.27	576.25	839.41	847.43	847.39	
VVEQMC[+57]ITQYER	2	y5	1	778.37	783.37	786.84	696.33	706.34	705.30	y5
	2	y7	1	778.37	783.37	786.84	969.45	979.45	980.41	
	2	y8	1	778.37	783.37	786.84	1100.49	1110.49	1112.45	
VVEQM[+16]C[+57]ITQYER	2	y5	1	786.36	791.37	794.84	696.33	706.34	705.30	y5
	2	y7	1	786.36	791.37	794.84	969.45	979.45	980.41	
	2	y8	1	786.36	791.37	794.84	1116.48	1126.49	1128.45	
ESQAYYQR	2	y3	1	522.74	527.75	529.22	466.24	476.25	473.22	y3

peptide modified sequence	precursor charge	fragment ion	product charge	precursor mz [light]	precursor mz [heavy]	precursor mz [$_{15}$N]	product mz [light]	product mz [heavy]	product mz [15n]	best fragment ion
	2	y4	1	522.74	527.75	529.22	629.30	639.31	637.28	
	2	y5	1	522.74	527.75	529.22	700.34	710.35	709.31	
	2	y5	1	756.86	760.87	n/a	667.34	675.36	n/a	y5
VVEQMC[+57]VTQYQK	2	y7	1	756.86	760.87	n/a	926.44	934.45	n/a	
	2	y8	1	756.86	760.87	n/a	1057.48	1065.49	n/a	
	2	y5	1	764.86	768.87	n/a	667.34	675.36	n/a	y5
VVEQM[+16]C[+57]VTQYQK	2	y7	1	764.86	768.87	n/a	926.44	934.45	n/a	
	2	y8	1	764.86	768.87	n/a	1073.48	1081.49	n/a	
	2	y4	1	544.74	549.74	n/a	510.23	520.24	n/a	y4
ESQAYYDGR	2	y5	1	544.74	549.74	n/a	673.29	683.30	n/a	
	2	y6	1	544.74	549.74	n/a	744.33	754.34	n/a	
	2	y5	1	764.36	768.37	n/a	668.32	676.34	n/a	y5
VVEQMC[+57]ITQYEK	2	y7	1	764.36	768.37	n/a	941.44	949.45	n/a	
	2	y8	1	764.36	768.37	n/a	1072.48	1080.49	n/a	
	2	y5	1	772.36	776.37	n/a	668.32	676.34	n/a	y5
VVEQM[+16]C[+57]ITQYEK	2	y7	1	772.36	776.37	n/a	941.44	949.45	n/a	
	2	y8	1	772.36	776.37	n/a	1088.48	1096.49	n/a	

Table S1B. Precursor and product ions monitored by LC-MRM-MS for Bovine 6 Protein Mix peptides.

Compound	Precursor (m/z)	Product (m/z)	Collision Energy (V)
DGGIDPLVR	471.256174	387.27143	18.3
DGGIDPLVR	471.256174	484.324194	18.3
DGGIDPLVR	471.256174	599.351137	18.3
DGGIDPLVR	471.256174	712.435201	18.3
DGGIDPLVR	471.256174	769.456664	18.3
YNLGLDLR	482.266541	403.229959	18.7
YNLGLDLR	482.266541	516.314023	18.7
YNLGLDLR	482.266541	573.335487	18.7
YNLGLDLR	482.266541	686.419551	18.7
YNLGLDLR	482.266541	800.462478	18.7
VLDALDSIK	487.281857	347.228896	18.9
VLDALDSIK	487.281857	462.255839	18.9

Compound	Precursor (m/z)	Product (m/z)	Collision Energy (V)
VLDALDSIK	487.281857	575.339903	18.9
VLDALDSIK	487.281857	646.377017	18.9
VLDALDSIK	487.281857	761.40396	18.9
GFC[+58.0]GLSQPK	497.736759	244.165568	19.2
GFC[+58.0]GLSQPK	497.736759	459.256174	19.2
GFC[+58.0]GLSQPK	497.736759	572.340238	19.2
GFC[+58.0]GLSQPK	497.736759	629.361701	19.2
GFC[+58.0]GLSQPK	497.736759	790.376365	19.2
VLVLDTDYK	533.294964	425.203075	20.4
VLVLDTDYK	533.294964	526.250754	20.4
VLVLDTDYK	533.294964	641.277697	20.4
VLVLDTDYK	533.294964	754.361761	20.4
VLVLDTDYK	533.294964	853.430175	20.4
TAAYVNAIEK	540.290213	389.239461	20.7
TAAYVNAIEK	540.290213	574.319502	20.7
TAAYVNAIEK	540.290213	673.387916	20.7
TAAYVNAIEK	540.290213	836.451245	20.7
TAAYVNAIEK	540.290213	907.488358	20.7
LVNELTEFAK	582.318971	365.218332	22.1
LVNELTEFAK	582.318971	595.308603	22.1
LVNELTEFAK	582.318971	708.392667	22.1
LVNELTEFAK	582.318971	837.43526	22.1
LVNELTEFAK	582.318971	951.478188	22.1
VGPLLAC[+58.0]LLGR	585.339183	458.308544	22.2
VGPLLAC[+58.0]LLGR	585.339183	619.323207	22.2
VGPLLAC[+58.0]LLGR	585.339183	690.360321	22.2
VGPLLAC[+58.0]LLGR	585.339183	803.444385	22.2
VGPLLAC[+58.0]LLGR	585.339183	916.528449	22.2
C[+58.0]AVVDVPFGGAK	610.802631	332.192845	23.1
C[+58.0]AVVDVPFGGAK	610.802631	576.314023	23.1
C[+58.0]AVVDVPFGGAK	610.802631	675.382437	23.1
C[+58.0]AVVDVPFGGAK	610.802631	790.40938	23.1
C[+58.0]AVVDVPFGGAK	610.802631	889.477794	23.1
YSTDVSVDEVK	621.298432	490.250754	23.4
YSTDVSVDEVK	621.298432	676.351196	23.4
YSTDVSVDEVK	621.298432	775.41961	23.4
YSTDVSVDEVK	621.298432	890.446553	23.4
YSTDVSVDEVK	621.298432	991.494232	23.4
YLGYLEQLLR	634.355888	529.345657	23.9
YLGYLEQLLR	634.355888	658.38825	23.9

Compound	Precursor (m/z)	Product (m/z)	Collision Energy (V)
YLGYLEQLLR	634.355888	771.472314	23.9
YLGYLEQLLR	634.355888	934.535643	23.9
YLGYLEQLLR	634.355888	991.557107	23.9
HLVDEPQNLIK	653.361701	487.323859	24.5
HLVDEPQNLIK	653.361701	712.435201	24.5
HLVDEPQNLIK	653.361701	841.477794	24.5
HLVDEPQNLIK	653.361701	956.504737	24.5
HLVDEPQNLIK	653.361701	1055.573151	24.5
FFVAPFPEVFGK	692.868631	351.202681	25.8
FFVAPFPEVFGK	692.868631	676.366452	25.8
FFVAPFPEVFGK	692.868631	920.48763	25.8
FFVAPFPEVFGK	692.868631	991.524744	25.8
FFVAPFPEVFGK	692.868631	1090.593158	25.8
SLHTLFGDELC[+58.0]K	710.842484	421.211531	26.5
SLHTLFGDELC[+58.0]K	710.842484	722.302531	26.5
SLHTLFGDELC[+58.0]K	710.842484	869.370945	26.5
SLHTLFGDELC[+58.0]K	710.842484	982.455009	26.5
SLHTLFGDELC[+58.0]K	710.842484	1083.502688	26.5
DDGSWEVIEGYR	713.317688	395.203744	26.5
DDGSWEVIEGYR	713.317688	524.246337	26.5
DDGSWEVIEGYR	713.317688	637.330401	26.5
DDGSWEVIEGYR	713.317688	736.398815	26.5
DDGSWEVIEGYR	713.317688	865.441408	26.5
IHGFDLAAINLQR	734.406975	714.425699	27.3
IHGFDLAAINLQR	734.406975	785.462812	27.3
IHGFDLAAINLQR	734.406975	898.546876	27.3
IHGFDLAAINLQR	734.406975	1013.573819	27.3
IHGFDLAAINLQR	734.406975	1217.663697	27.3
LGEYGFQNALIVR	740.401358	387.27143	27.5
LGEYGFQNALIVR	740.401358	685.435535	27.5
LGEYGFQNALIVR	740.401358	813.494113	27.5
LGEYGFQNALIVR	740.401358	960.562526	27.5
LGEYGFQNALIVR	740.401358	1017.58399	27.5
LSFNPTQLEEQC[+58.0]HI	858.898519	430.17548	31.5
LSFNPTQLEEQC[+58.0]HI	858.898519	687.276651	31.5
LSFNPTQLEEQC[+58.0]HI	858.898519	816.319244	31.5
LSFNPTQLEEQC[+58.0]HI	858.898519	929.403308	31.5
LSFNPTQLEEQC[+58.0]HI	858.898519	1255.562328	31.5
IVGYLDEEGVLDQNR	860.431041	417.220457	31.5
IVGYLDEEGVLDQNR	860.431041	532.2474	31.5

Compound	Precursor (m/z)	Product (m/z)	Collision Energy (V)
IVGYLDEEGVLDQNR	860.431041	645.331464	31.5
IVGYLDEEGVLDQNR	860.431041	801.421342	31.5
IVGYLDEEGVLDQNR	860.431041	1174.533471	31.5
HGGTIPIVPTAEFQDR	869.449568	565.272886	31.8
HGGTIPIVPTAEFQDR	869.449568	963.453036	31.8
HGGTIPIVPTAEFQDR	869.449568	1062.52145	31.8
HGGTIPIVPTAEFQDR	869.449568	1272.658277	31.8
HGGTIPIVPTAEFQDR	869.449568	1385.742341	31.8
YNGVFQEC[+58.0]C[+58.0]QAEDK	875.340176	751.292695	32
YNGVFQEC[+58.0]C[+58.0]QAEDK	875.340176	912.307358	32
YNGVFQEC[+58.0]C[+58.0]QAEDK	875.340176	1041.349951	32
YNGVFQEC[+58.0]C[+58.0]QAEDK	875.340176	1169.408529	32
YNGVFQEC[+58.0]C[+58.0]QAEDK	875.340176	1316.476943	32
C[+58.0]VAVGESDGSIWNPDGIDPK	1058.978226	244.165568	38.3
C[+58.0]VAVGESDGSIWNPDGIDPK	1058.978226	529.298038	38.3
C[+58.0]VAVGESDGSIWNPDGIDPK	1058.978226	741.377745	38.3
C[+58.0]VAVGESDGSIWNPDGIDPK	1058.978226	855.420673	38.3
C[+58.0]VAVGESDGSIWNPDGIDPK	1058.978226	1041.499986	38.3

Table S1C. Precursor and product ions monitored by LC-MRM-MS for PRTC peptides.

Compound	Precursor (m/z)	Product (m/z)	Collision Energy (V)
SSAAPPPPPR	493.7683	899.497296	17.2
SSAAPPPPPR	493.7683	812.465268	17.2
SSAAPPPPPR	493.7683	741.428154	17.2
SSAAPPPPPR	493.7683	670.39104	17.2
SSAAPPPPPR	493.7683	573.338276	17.2
SSAAPPPPPR	493.7683	476.285512	17.2
SSAAPPPPPR	493.7683	379.232748	17.2
GISNEGQNASIK	613.316765	1168.604791	22
GISNEGQNASIK	613.316765	1055.520727	22
GISNEGQNASIK	613.316765	968.488698	22
GISNEGQNASIK	613.316765	854.445771	22
GISNEGQNASIK	613.316765	725.403178	22
GISNEGQNASIK	613.316765	668.381714	22
GISNEGQNASIK	613.316765	540.323136	22
GISNEGQNASIK	613.316765	426.280209	22
HVLTSIGEK	496.286748	854.507309	17.3
HVLTSIGEK	496.286748	755.438895	17.3

Compound	Precursor (m/z)	Product (m/z)	Collision Energy (V)
HVLTSIGEK	496.286748	642.354831	17.3
HVLTSIGEK	496.286748	541.307152	17.3
HVLTSIGEK	496.286748	454.275124	17.3
HVLTSIGEK	496.286748	341.19106	17.3
DIPVPKPK	451.283477	786.532735	15.5
DIPVPKPK	451.283477	673.448671	15.5
DIPVPKPK	451.283477	576.395907	15.5
DIPVPKPK	451.283477	477.327494	15.5
DIPVPKPK	451.283477	380.27473	15.5
DIPVPKPK	451.283477	252.179767	15.5
IGDYAGIK	422.73636	731.38138	14.4
IGDYAGIK	422.73636	674.359916	14.4
IGDYAGIK	422.73636	559.332973	14.4
IGDYAGIK	422.73636	396.269644	14.4
IGDYAGIK	422.73636	325.23253	14.4
TASEFDSAIAQDK	695.832445	1289.609936	25.3
TASEFDSAIAQDK	695.832445	1218.572822	25.3
TASEFDSAIAQDK	695.832445	1131.540794	25.3
TASEFDSAIAQDK	695.832445	1002.4982	25.3
TASEFDSAIAQDK	695.832445	855.429786	25.3
TASEFDSAIAQDK	695.832445	740.402843	25.3
TASEFDSAIAQDK	695.832445	653.370815	25.3
TASEFDSAIAQDK	695.832445	582.333701	25.3
SAAGAFGPELSR	586.800329	1085.561353	20.9
SAAGAFGPELSR	586.800329	1014.524239	20.9
SAAGAFGPELSR	586.800329	943.487125	20.9
SAAGAFGPELSR	586.800329	886.465662	20.9
SAAGAFGPELSR	586.800329	815.428548	20.9
SAAGAFGPELSR	586.800329	668.360134	20.9
SAAGAFGPELSR	586.800329	611.33867	20.9
SAAGAFGPELSR	586.800329	514.285906	20.9
SAAGAFGPELSR	586.800329	385.243313	20.9
ELGQSGVDTYLQTK	773.895577	1417.741284	28.4
ELGQSGVDTYLQTK	773.895577	1304.65722	28.4
ELGQSGVDTYLQTK	773.895577	1247.635757	28.4
ELGQSGVDTYLQTK	773.895577	1119.577179	28.4
ELGQSGVDTYLQTK	773.895577	1032.545151	28.4
ELGQSGVDTYLQTK	773.895577	975.523687	28.4
ELGQSGVDTYLQTK	773.895577	876.455273	28.4
ELGQSGVDTYLQTK	773.895577	761.42833	28.4

Compound	Precursor (m/z)	Product (m/z)	Collision Energy (V)
ELGQSGVDTYLQTK	773.895577	660.380651	28.4
GLILVGGYGTR	558.325982	1058.623225	19.8
GLILVGGYGTR	558.325982	945.539161	19.8
GLILVGGYGTR	558.325982	832.455097	19.8
GLILVGGYGTR	558.325982	719.371033	19.8
GLILVGGYGTR	558.325982	620.302619	19.8
GLILVGGYGTR	558.325982	563.281155	19.8
GLILVGGYGTR	558.325982	506.259692	19.8
GILFVGSGVSGGEEGAR	801.411503	1431.710202	29.4
GILFVGSGVSGGEEGAR	801.411503	1318.626138	29.4
GILFVGSGVSGGEEGAR	801.411503	1171.557724	29.4
GILFVGSGVSGGEEGAR	801.411503	1072.48931	29.4
GILFVGSGVSGGEEGAR	801.411503	1015.467847	29.4
GILFVGSGVSGGEEGAR	801.411503	928.435818	29.4
GILFVGSGVSGGEEGAR	801.411503	871.414354	29.4
GILFVGSGVSGGEEGAR	801.411503	772.34594	29.4
GILFVGSGVSGGEEGAR	801.411503	685.313912	29.4
SFANQPLEVVYSK	745.392473	1402.745641	27.2
SFANQPLEVVYSK	745.392473	1255.677227	27.2
SFANQPLEVVYSK	745.392473	1184.640114	27.2
SFANQPLEVVYSK	745.392473	1070.597186	27.2
SFANQPLEVVYSK	745.392473	942.538609	27.2
SFANQPLEVVYSK	745.392473	845.485845	27.2
SFANQPLEVVYSK	745.392473	732.401781	27.2
SFANQPLEVVYSK	745.392473	603.359188	27.2
LTILEELR	498.801809	883.512278	17.4
LTILEELR	498.801809	782.464599	17.4
LTILEELR	498.801809	669.380535	17.4
LTILEELR	498.801809	556.296471	17.4
LTILEELR	498.801809	427.253878	17.4
LTILEELR	498.801809	298.211285	17.4
NGFILDGFPR	573.302507	1031.554811	20.4
NGFILDGFPR	573.302507	974.533347	20.4
NGFILDGFPR	573.302507	827.464933	20.4
NGFILDGFPR	573.302507	714.380869	20.4
NGFILDGFPR	573.302507	601.296805	20.4
NGFILDGFPR	573.302507	486.269862	20.4
NGFILDGFPR	573.302507	429.248399	20.4

Table S2. Species sequence matching, sequence context, and pilot study detection of all peptides monitored.

previous AA	sequence	next AA	species	MS peak area in recombinant PrP	peak area in CSF
(LCKK)	RPKPGGWNTGGSR	(YPGQ)	human, cyno, mouse, rat	5.49E+09	1.24E+08
(GGSR)	YPGQGSPGGNR	(YPP)	human, cyno, mouse, rat	4.90E+10	8.62E+08
(AMSR)	PIIHFGSDYEDR	(YYR)	human		1.06E+09
(TTTK)	GENFTETDVK	(MME)	human, cyno, mouse, rat	5.11E+10	2.48E+08
(MMER)	VVEQMCITQYER	(ESQ)	human	3.46E+09	1.12E+09
(MMER)	VVEQMCVTQYQK	(ESQA)	mouse, rat	5.21E+10	
(MMER)	VVEQMCITQYEK	(ESQ)	cyno		
(QYER)	ESQAYYQR	(GSS)	human, cyno	2.32E+10	
(QYQK)	ESQAYYDGR	(RSS)	mouse, rat	6.85E+10	

Table S3. Normalization of peptide responses. *The L, $_{15}$N, and L:$_{15}$N columns summarize the data from Figure 2. Across N=55 clinical samples, the mean L:$_{15}$N ratio for each peptide varied by >10-fold. If these ratios are simply multiplied by the known concentration of $_{15}$N protein spiked in (24 ng/mL), they correspond to "raw" PrP concentrations here, ranging from 39 – 478 ng/mL. We calculated a response factor for each peptide as described in Methods and Figure S8, which, for the one CSF sample used in the dose-response experiment, serves to bring each peptide up to equal abundance as the highest-responding peptide (VVEQMCITQYER). Multiplying the L:$_{15}$N ratio by the response factor and the spiked $_{15}$N PrP concentration in clinical samples yields normalized PrP concentrations that are within ±50% of one another which represents the residual differences in peptide response between the clinical samples and the control sample used in the dose-response experiment.*

peptide	mean ± sd L peak area (millions)	mean ± sd $_{15}$N peak area (millions)	mean ± sd L:$_{15}$N ratio	mean raw [PrP] (ng/mL)	response factor	mean normalized [PrP] (ng/mL)
RPKPGGWNTGGSR	0.14±0.12	0.10±0.08	1.8±1.4	43	11.6	503
YPGQGSPGGNR	0.26±0.22	0.05±0.03	5.3±2.7	130	2.5	329
PIIHFGSDYEDR	1.59±1.04	0.10±0.05	16.7±9.3	409	1.2	497
GENFTETDVK	0.49±0.36	0.33±0.19	1.6±0.9	39	9.0	350
VVEQMCITQYER	3.67±3.17	0.20±0.15	19.7±10.7	478	1.0	478
ESQAYYQR	0.35±0.28	0.08±0.05	4.8±3.3	116	3.2	373

Table S4. Characteristics and performance of the six PrP MRM human peptides in clinical samples by quartile. *For each peptide, the N=55 samples were broken into quartiles of L:$_{15}$N ratio. The mean coefficient of variation (CV) of technical duplicates and the mean L:$_{15}$N ratio of samples was calculated within each quartile. Note that the rank order used for binning is similar (Figure 3B) but not identical between peptides. Also note that for VVEQMCITQYER, because 12 replicates (including both replicates of one sample) with methionine oxidation were thrown out, sample size is N=44 for CV calculations (using only those samples with N=2 valid process replicates) and N=54 for mean L:$_{15}$N ratio calculations (including all samples with N≥1 valid process replicate). The results show that all six peptides, across all four quartiles, had mean CV ≤15% and mean L:$_{15}$N ratio ≥0.6. Because our data suggest assay linearity extending at least as low as 0.1x of the $_{15}$N PrP concentration we used (estimated to be 0.24 ng/mL, Figure S5C), this suggests that PrP MRM had acceptable performance in all quartiles and that all measurements in clinical samples were within the dynamic range of the assay.*

	mean CV by quartile				mean L:$_{15}$N ratio by quartile			
peptide	**0-24%**	**25-49%**	**50-74%**	**75-100%**	**0-24%**	**25-49%**	**50-74%**	**75-100%**
RPKPGGWNTGGSR	9.8%	14.5%	11.7%	3.9%	0.7	1.2	1.8	3.7
YPGQGSPGGNR	12.5%	11.9%	14.0%	9.5%	2.5	4.1	5.9	9.3
PIIHFGSDYEDR	10.9%	11.3%	5.4%	11.1%	7.9	11.9	17.8	30.9
GENFTETDVK	12.1%	9.9%	8.8%	6.6%	0.6	1.2	1.8	2.9
VVEQMCITQYER	12.8%	12.0%	3.4%	6.4%	9.0	14.9	21.7	35.6
ESQAYYQR	9.2%	9.3%	10.7%	9.1%	2.0	3.1	4.8	9.6

Table S5. Characteristics and performance of the nine PrP MRM peptides in assay development samples. *Analytical validation experiments were performed without $_{15}$N protein internal controls and instead utilized the light:heavy peptide area under the curve ratio as described in Methods. Data from N=19 samples (N=4 cynomolgous macaque CSF, N=10 human CSF, N=1 human brain, N=1 mouse brain, and N=4 rat CSF) in a total of N=35 replicates were analyzed to determine the basic performance characteristics of each peptide (this table) as well as the sensitivity and selectivity of the assay (Figure S5). Here, only data from samples where the peptide is sequence-matched to the species in question are shown. *Reduced peptides only; met-ox versions were not monitored in these runs. Retention time is shown as mean±sd in minutes for a 45-minute gradient. Mean L:H ratio is the mean light:heavy area ratio. Mean CV is calculated across the subset of samples run in process duplicate or triplicate within the same run, and N indicates the number of unique samples.*

peptide	retention time (min)	mean L:H ratio	mean CV
RPKPGGWNTGGSR	16.9±0.7 (N=28)	0.1 (N=21)	11% (N=12)
YPGQGSPGGNR	18.6±0.7 (N=28)	0.6 (N=21)	5.2% (N=12)
PIIHFGSDYEDR	36.5±1.8 (N=19)	3.9 (N=13)	6.5% (N=9)
GENFTETDVK	26.7±1.3 (N=28)	0.4 (N=21)	7.2% (N=12)
VVEQMCITQYER*	37.0±1.5 (N=19)	7.0 (N=13)	5.7% (N=9)
VVEQMCVTQYQK*	33.7±0.6 (N=3)	1.0 (N=4)	7.2% (N=1)
VVEQMCITQYEK*	35.3±0.3 (N=6)	1.4 (N=2)	4.3% (N=2)
ESQAYYQR	19.9±0.8 (N=25)	2.2 (N=17)	3.3% (N=11)
ESQAYYDGR	23.3±0.3 (N=3)	0.3 (N=4)	0.92% (N=1)

SUPPLEMENTAL FIGURES

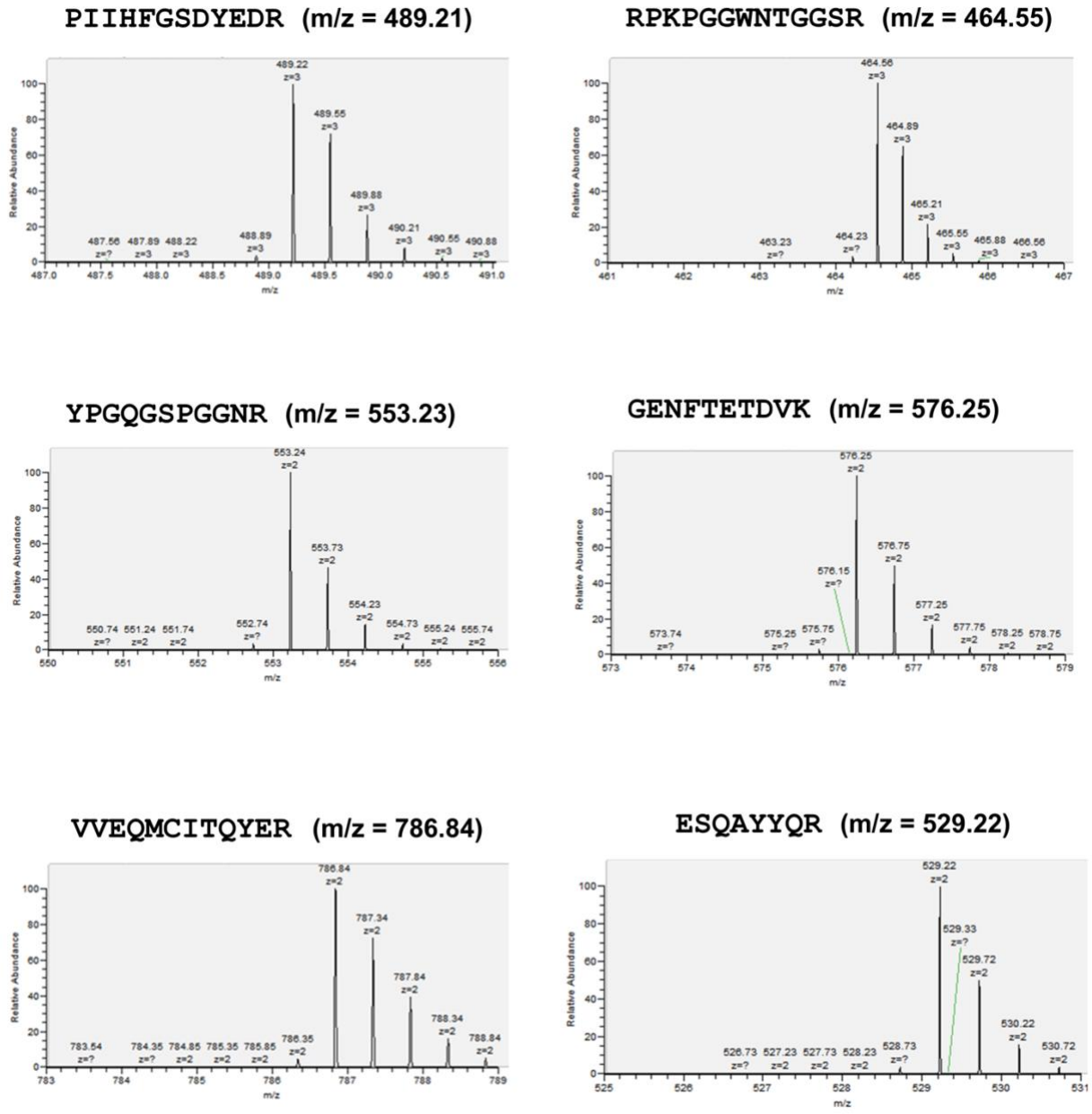

Figure S1. Extracted MS intensities for human PrP peptides used for estimation of isotopic purity of ^{15}N-labeled protein. *Isotopic envelopes of each peptide identified by MS/MS after digestion of the ^{15}N protein with trypsin. Minimal or lack of observed mz peak areas less than the ^{12}C monoisotopic mass peak (highest signal for the mz of these peptides) indicates near complete ^{15}N incorporation. Lower mass peaks corresponding to incomplete ^{15}N incorporation were unquantifiably small, consistent with >97.5% isotopic purity for all peptides.*

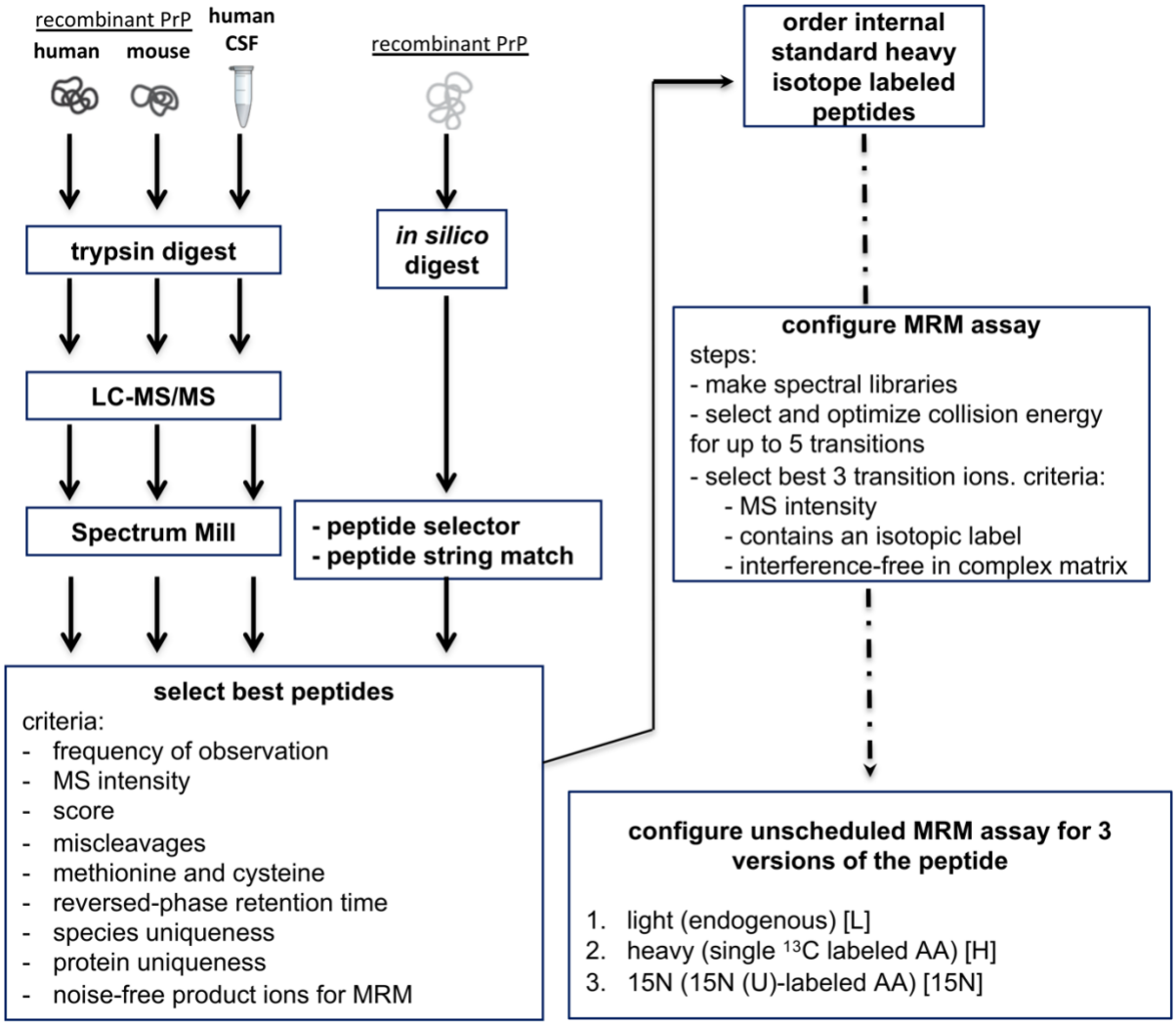

Figure S2. Assay development workflow. *Schematic outline of steps described in Methods to select peptides based on empirical and bioinformatic data, and optimize and configure a 9-plex MRM assay.*

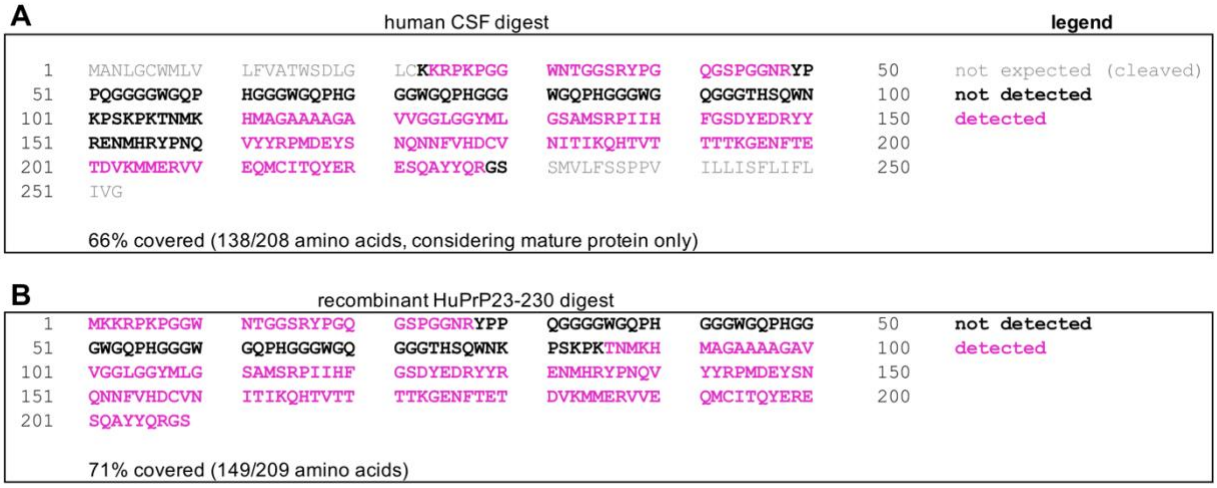

Figure S3. Sequence coverage map. *Map of sequence coverage of PrP in pilot LC-MS/MS analyses of* ***A)*** *human CSF and* ***B)*** *recombinant HuPrP23-230. A peptide containing a retained N-terminal methionine (MKKRPKPGGWNTGGSR) was detected in the recombinant digest with intensity* 6.9×10^9.

```
                                                                                                    amino acid
human         MANLGCWMLV LFVATWSDLG LCKKRPKPGG WNTGGSRYPG QGSPGGNRYP PQGGGGWGQP      60
cynomolgus    MANLGCWMLV LFVATWSDLG LCKKRPKPGG WNTGGSRYPG QGSPGGNRYP PQGGGGWGQP      60
mouse         MANLGYWLLA LFVTMWTDVG LCKKRPKPGG WNTGGSRYPG QGSPGGNRYP PQ-GGTWGQP      59
rat           MANLGYWLLA LFVTTCTDVG LCKKRPKPGG WNTGGSRYPG QGSPGGNRYP PQSGGTWGQP      60
              ***** *:*. ***:  :*:* ********** ********** ********** ** ** ****

human         HGGGWGQPHG GGWGQPHGGG WGQPHGGGWG QGGGTHSQWN KPSKPKTNMK HMAGAAAAGA     120
cynomolgus    HGGGWGQPHG GGWGQPHGGG WGQPHGGGWG QGGGTHNQWH KPSKPKTSMK HMAGAAAAGA     120
mouse         HGGGWGQPHG GSWGQPHGGS WGQPHGGGWG QGGGTHNQWN KPSKPKTNLK HVAGAAAAGA     119
rat           HGGGWGQPHG GGWGQPHGGG WGQPHGGGWS QGGGTHNQWN KPSKPKTNLK HVAGAAAAGA     120
              ********** *.*******. *********. ******.**: *******.:* *:********

human         VVGGLGGYML GSAMSRPIIH FGSDYEDRYY RENMHRYPNQ VYYRPMDEYS NQNNFVHDCV     180
cynomolgus    VVGGLGGYML GSAMSRPLIH FGNDYEDRYY RENMYRYPNQ VYYRPVDQYS NQNNFVHDCV     180
mouse         VVGGLGGYML GSAMSRPMIH FGNDWEDRYY RENMYRYPNQ VYYRPVDQYS NQNNFVHDCV     179
rat           VVGGLGGYML GSAMSRPMLH FGNDWEDRYY RENMYRYPNQ VYYRPVDQYS NQNNFVHDCV     180
              ********** *******::* **.*:***** ****:***** *****:*:** **********

human         NITIKQHTVT TTTKGENFTE TDVKMMERVV EQMCITQYER ESQAYYQ--R GSSMVLFSSP     238
cynomolgus    NITIKQHTVT TTTKGENFTE TDVKMMERVV EQMCITQYEK ESQAYYQ--R GSSMVLFSSP     238
mouse         NITIKQHTVT TTTKGENFTE TDVKMMERVV EQMCVTQYQK ESQAYYDGRR SSSTVLFSSP     239
rat           NITIKQHTVT TTTKGENFTE TDVKMMERVV EQMCVTQYQK ESQAYYDGRR SS-AVLFSSP     239
              ********** ********** ********** ****:***:: ******:  * .*  ******

human         PVILLISFLI FLIVG                                                      253
cynomolgus    PVILLISFLI FLIVG                                                      253
mouse         PVILLISFLI FLIVG                                                      254
rat           PVILLISFLI FLIVG                                                      254
              ********** *****
```

Figure S4. Selected PrP peptides in protein multiple alignment context. *Full amino acid sequences of PrP for the four species of interest with locations of PrP MRM peptides noted in bold colors. Bold indicates residues present in the mature, post-translationally modified protein. The grayed out N terminus is an ER signal peptide and the grayed out C terminus is a GPI signal; both are cleaved before the protein reaches the cell surface. The mature protein is ~23 kDa, see Methods in main text. For human and mouse PrP, the non-gray text also corresponds to the residues present in the recombinant PrP constructs used in this study. Sequences from UniProt: P04156 (human), P67992 (cynomolgus macaque), P04925 (mouse), P13852 (rat), aligned with Clustal O 1.2.4 (see Methods).*

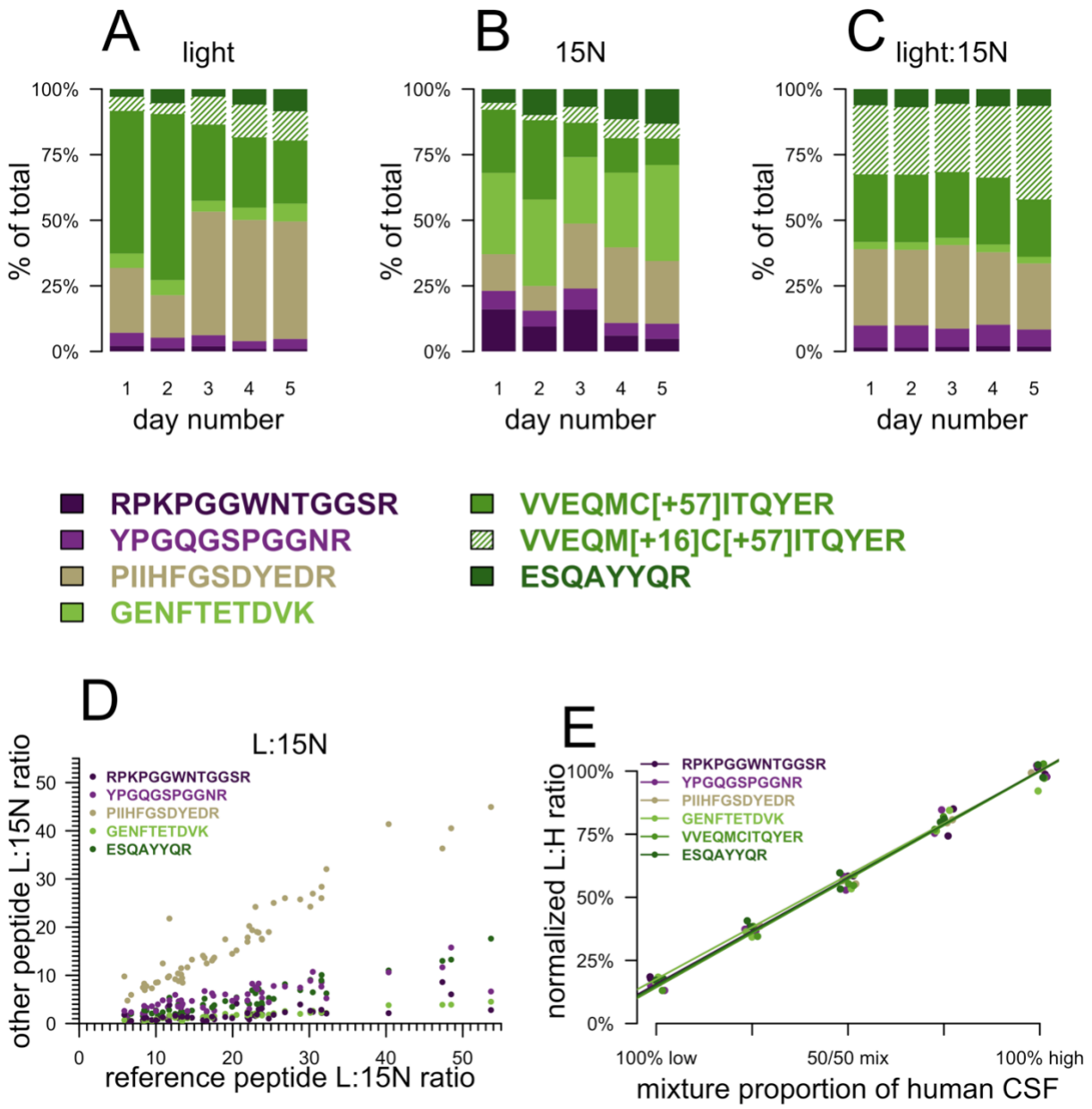

Figure S5. Quality control and partial analytical validation of the PrP MRM assay. A-C) *Peptide abundance and ratios by day. Each stacked barplot shows the percent of total PrP peptide abundance contributed by each peptide in clinical samples across five different days.* ***D)*** *Scatterplot correlations for L:$_{15}$N ratio between peptides across clinical samples. The most abundant peptide, VVEQMCITQYER, is used as reference (x axis) versus all other peptides (y axis). The slopes differ, consistent with different response of different peptides (Table S3 and Figure 2 and S6), but linear correlations are observed for each, across the full dynamic range of samples analyzed. This provides supporting evidence that our assay is technically able to measure the biological variability among samples, and that all peptides move together according to changes in disease state.* ***E)*** *Dilution linearity validation of the assay. Two human CSF samples previously measured to have high (240 ng/mL) and low (12 ng/mL) PrP by ELISA were mixed in different proportions (all low, 25/75, 50/50, 75/25, and all high) and assayed by PrP MRM. Each peptide's light:heavy ratio is normalized to the average value of the two "all high" replicates, and best-fit lines are shown. Individual replicates are jittered slightly along the*

x-axis so that separate points are visible. Each peptide exhibits good linearity. Note that because the low-PrP CSF sample still has non-zero PrP, the fact that the y-intercepts are non-zero is expected. Best fit lines for each peptide have adjusted R_2 values ranging 97.6% - 99.8% (linear regression).

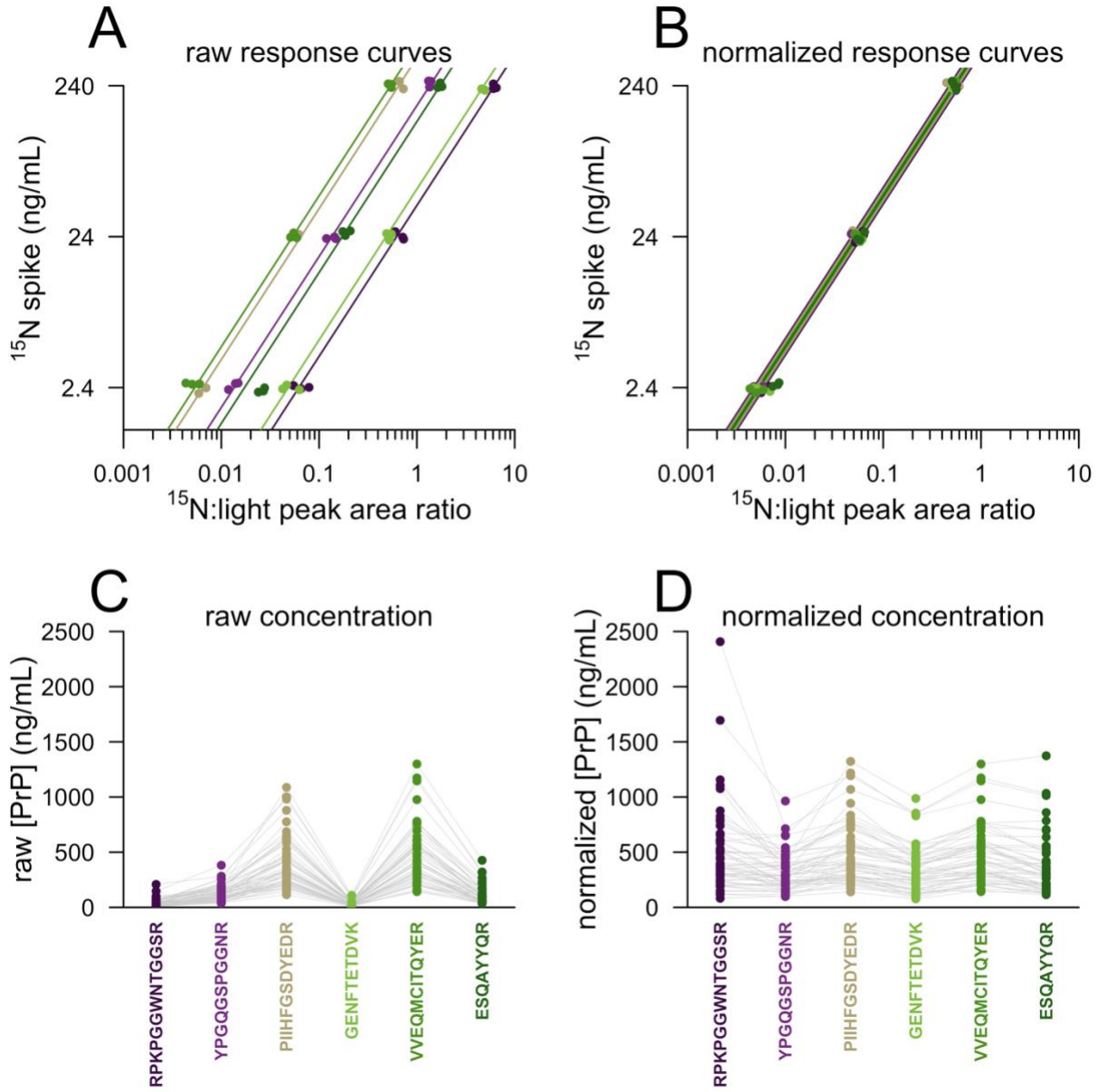

Figure S6. Normalization based on dose-response data. *Normalization was performed as described in Methods using data from the same ^{15}N dose-response experiment depicted in Figure S5C.* ***A)*** *Spiked ^{15}N PrP concentration versus observed ^{15}N:L ratio for each peptide. Each point is one replicate, and points are jittered along the y axis so that each point is visible. We fit linear models correlating spike ~ ^{15}N:L ratio with the y-intercept fixed at zero, and each peptide yielded a different slope. Note that this figure is plotted in log-log space, so the different slopes appear as different intercepts. We assigned each peptide a response factor equal to the maximum observed slope (that for VVEQMITQYER, top left) divided by its own slope.* ***B)*** *Same data from panel A but with response factors applied.* ***C)*** *Raw PrP concentrations in clinical samples (simply ^{15}N:L ratio times the known ^{15}N concentration of 24 ng/mL).* ***D)*** *Normalized PrP concentrations in clinical samples (^{15}N:L ratio times 24 ng/mL times peptide response factor). In C and D, gray lines connect the dots representing distinct peptides from the same sample.*

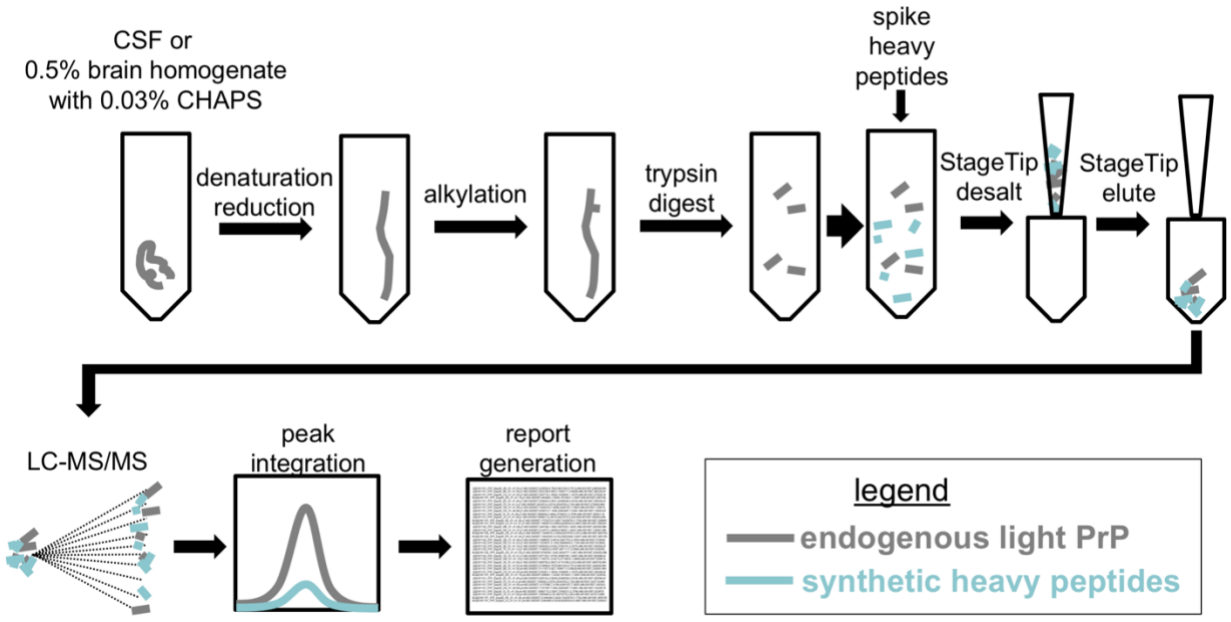

Figure S7. PrP MRM workflow for application to preclinical species. *The workflow is the same as in Figure 1B but with CSF or brain homogenate as input, and with synthetic single residue* $_{15}N/_{13}C$ *labeled heavy peptides addead after trypsin digest instead of fully* $_{15}N$*-labeled recombinant added at the beginning.*